ABSTRACT

BAGAL, ABHIJEET SUBHASHRAO. Fabrication of Subwavelength Periodic Nanostructures using Immersion Interference Lithography. (Under the direction of committee chair Dr. Chih-Hao Chang).

Immersion lithography is being extensively used in the semiconductor industry to make high resolution structures, by taking the advantage of higher refractive index of immersion fluids. Recent efforts in this field are focused on making high resolution periodic nanostructures by combining immersion lithography with interference lithography. The available methods suffer from operational difficulties, high setup cost and high spatial-phase distortion. In this work, we present a new design to address these problems, by combining the immersion lithography with Lloyd's mirror interferometer.

Using the design proposed in this work, we have successfully fabricated a structure having periodicity of 112 nm using light of 325 nm wavelength. With this setup, it is possible to fabricate the structure over a macroscopic region. The system proposed in this work is very flexible and we can get any desired period over a range by making simple adjustments. We have been able to make structures with periodicity ranging from 112 nm to 170 nm using two different immersion fluids and light of 325 nm wavelength.

With this setup, it is possible to fabricate structure having even smaller period, by using an immersion fluid with higher refractive index or by using smaller wavelength of light. We also present the effect of absorption of light by immersion fluid, on the quality of the structure produced. For small samples, it is possible to fabricate structure with low spatial-phase distortion, as the difference in the relative distance travelled by two interfering

beams is small. By using the immersion fluids having smaller absorption coefficient, it is possible to fabricate the structures over a very large area, with high spatial coherence.

Future work involves making use of this system to fabricate 2D structures in the photoresist, which will act as a mask during RIE process. By making use of RIE, the 2D structure will be replicated into the substrate, to produce densely packed Nano cones. This structure will have better superhydropobic/philic property, improved antireflection and higher surface to volume ratio.

Fabrication of Subwavelength Periodic Nanostructures using Immersion Interference Lithography

by
Abhijeet Subhashrao Bagal

A thesis submitted to the Graduate Faculty of
North Carolina State University
in partial fulfillment of the
requirements for the degree of
Master of Science

Mechanical Engineering

Raleigh, North Carolina

2012

APPROVED BY:

_____	_____
Dr. Xiaoning Jiang	Dr. Yong Zhu

_____
Dr. Chih-Hao Chang
Chair of Advisory Committee

DEDICATION

In memory of my mother Vidya, who has been with me every step of the way.

BIOGRAPHY

Abhijeet Bagal is from Latur, a city in Southern Maharashtra. It is located in central India and has been blessed with a mild weather conducive for learning and education. One of the most developed cities in Southern Maharashtra; it attracts students from far and wide.

Abhijeet completed Bachelors in Mechanical Engineering in 2005 from SRTMU University in Latur. His love for scientific enquiry was instrumental in his decision to pursue Masters from North Carolina in Mechanical and Aerospace Engineering and he has decided to pursue PhD in this field.

He enjoys sports and likes to spend his free time in the company of family and friends.

ACKNOWLEDGMENTS

I would like to acknowledge my heartfelt gratitude to my Graduate advisor, Dr. Chih-Hao Chang for providing me with the opportunity to work under his expert guidance and for his persistent help without which this thesis would not have been possible. His genius and passion for research has inspired me to deliver my best. His knowledge and experience have been instrumental in overcoming the hurdles I faced in research.

I would also like to thank my lab mates Xu Zhang, Qiaoyin Yang, Jonathan Elek, WeiYi Chang and Jonathan Chu, with whom I have had insightful discussions for supporting me in research.

I express my sincere gratitude for the technical support I got from NCSU Nanofabrication Center and Analytical Instrumentation Facility.

Special thanks to my friends Arunesh Goswami, Aadhithya Hossali, Nilesh Rajule, Prasad Gandhi, Gerry Anthony, Sharavan Arcot, and many more, for providing the help and friendship that I needed.

I would also like to thank my family for all the love and support without which this thesis would not have been possible. Lastly, I would like to thank my fiancée Priyadarshini for being with me in all the ups and downs, and for making my life more beautiful.

TABLE OF CONTENTS

LIST OF TABLES

LIST OF FIGURES

Chapter 1 Introduction

The advent of nanotechnology over the last few decades has created a lot of interest in the research community in all fields of research. It has been observed that the structures at Nano scale behave very differently than its bulk counterpart. Researchers have been able to manipulate geometric and material properties of materials at Nano scale to get better performance characteristics than their bulk materials. This has been the source of increased curiosity and interest among researchers and engineers alike. And a wide applicability of this field has opened up new fields and interdisciplinary applications. Nanotechnology has a potential to create new materials and devices with applications in medical diagnosis, energy harvesting, electronics, micro robotics and ultrasensitive sensors.

Though the field of nanotechnology has great potential, it is quite challenging to make Micro/Nano scale devices with high precision over large areas. There are two different techniques followed, and the first is top-down approach. This approach is most commonly used for fabricating microprocessors with features smaller than 100 nm. Most commonly used top-down approach is optical lithography, which involves using short wavelength light source to replicate mask pattern. Another technique involving mechanical deformation of resist, called Nano imprinting, is also being used in the top down approach. With top-down approach, it is difficult to make structures having length scales below 10s of nanometer. This thesis will primarily follow the top-down approach using optical lithography.

The second technique in fabrication of Nano scaled devices is the bottom-up approach. It involves manipulation of individual Nano scale components, assembled together

to build complex structures [1, 2]. This method becomes very useful when the component size goes down. With bottom-up approach, it becomes difficult to control things as structures increase in size. It is difficult to maintain spatial-phase coherence over a large area using this approach. The two methods mentioned here are complimentary to each other.

1.1 Periodic Nanostructures:

Characteristics of periodic structures are more predictable than the randomly oriented structures and they can be better tailored to get the desired results. In case of periodic nanostructures, geometry of a material is repeated spatially over a period of Λ. For a 1D structure periodic in the *x*-direction, we have the relation;

$$f(x) = f(x + n\Lambda)$$

Where, *f(x)* is the material property of interest and *n* is an integer. Figure 1-1 shows the structure periodic in *x*-direction.

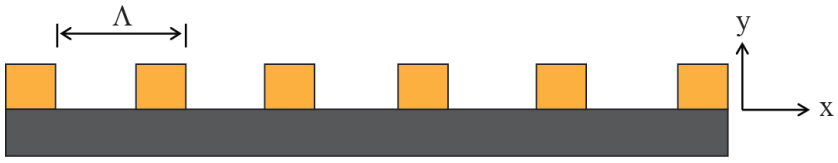

Figure 1-1: 1 D structure periodic in x-direction

Quality of periodic structures is characterized by three important parameters, which are; spatial resolution, spatial-phase coherence and pattern area. The first parameter, spatial

resolution, defines the feature size of the structure that can be produced with accuracy and repeatability. This parameter is the driving force behind the smaller and smaller devices. Features with dimensionality in the range of 10s of nanometer are being used in the semiconductor industry to accommodate increasing number of devices per unit area.

Spatial-phase coherence is the measure of accuracy for the periodicity of the structure. It describes a relative phase difference between the structures at different locations. A good periodic structure will have no relative phase error over a very large area. The third parameter is pattern area and it defines the area over which we have the usable desired nanostructured pattern. This parameter defines the success of any methodology used to fabricate the nanostructures as, the larger the area fabricated, the better is the method for commercial use. It, of course, involves the time and cost required to fabricate the structure. These three parameters are very useful in verifying the quality of nanostructures and emphasize can be given on either of these based on the required characteristics.

Periodic gratings of Nano scale find applications in x-ray [32, 27] and extreme ultraviolet [31] spectroscopy and also in atomic diffraction [29]. The nanostructures can also be used to enhance the antireflection properties of the surface [5] and to make the templates for sub assembly [26]. [30] Shows the use of Nano electrodes with flexible electronics to collect the information from a brain and also indicates that, by having densely packed electrodes, it is possible to improve the data collection process further.

Figure 1-2 shows few examples of periodic nanostructures. Image (a) shows 3D Nano lattice fabricated using self-assembly of Nano spheres. Image (b) shows use of Nano spheres to assemble nanoparticle catalysts for periodic carbon nanotube growth. Nano cones can be

used to provide gradient based refractive index to reduce reflection form a surface (c). Image (d) show 3D Micro/Nano structured material

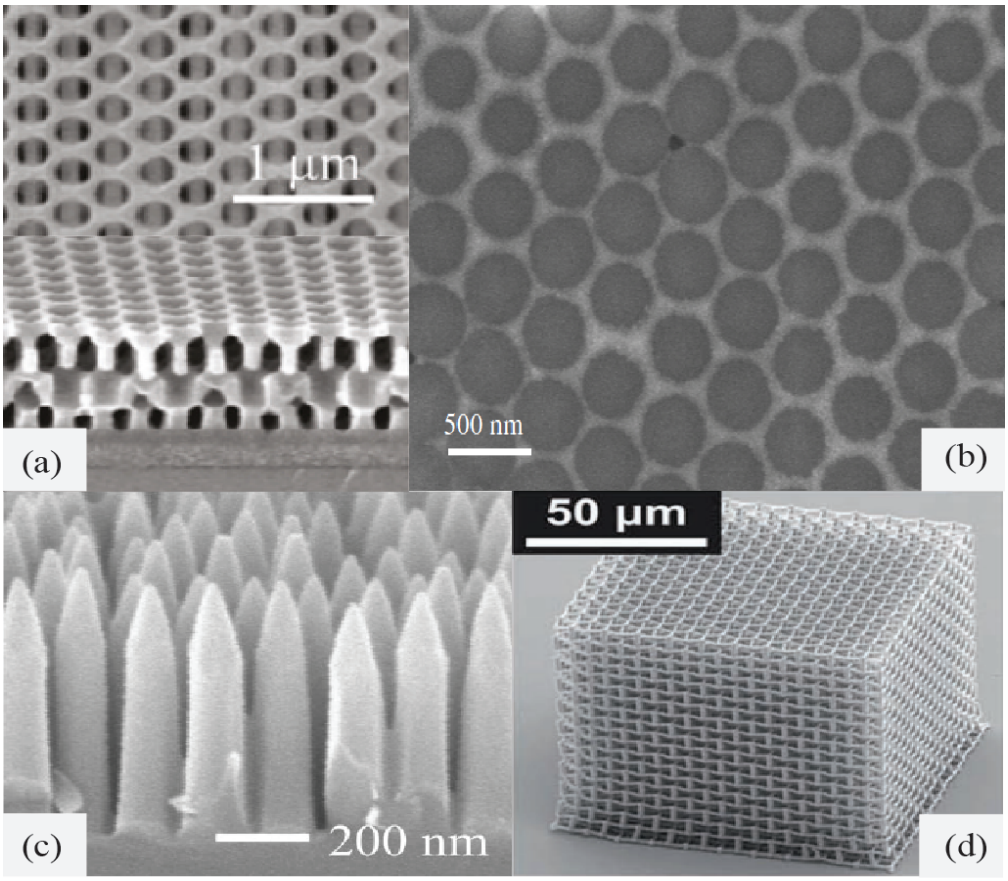

Figure 1-2: Periodic nanostructures (a) 3D structure using self-assembly [3] (b) Nanoparticle assembly using Nano spheres [4] (c) Sub wavelength 2D gratings with antireflection property [5] (d) 3D Micro\Nano structure material [6]

1.2 Methods for Nanostructure patterning:

Periodic nanostructures can be fabricated using many different methods, few of which are; probe based techniques, pattern transfer via physical contact, self-assembly and optical lithography.

Probe based technique covers all the lithography methods that use a small tip that is scanned over the substrate to write the pattern. Some of the examples of this method are; e-beam, ion beam, scanning tunneling microscope (STM) [7], atomic force microscope (AFM) [8], scanning electrochemical microscope (SECM) [9], near field scanning optical microscope (NSOM) [10], etc. These methods can provide very high resolution with arbitrary geometry. But these methods are very time consuming and are not suitable for mass production of nanostructures.

Techniques like; Nano imprinting, molding and embossing can be used to transfer the pattern via physical contact. These methods use a patterned mask which will is brought in physical contact with a UV or thermally curable material [11]. Due to the mask used, these methods are expensive and are also limited in the smallest possible feature size.

The process of self-assembly is an example of bottom-up approach of fabrication. This technique resembles the biological phenomenon by which proteins and DNA's are assembled together. In this, the sub-units are self-assembled together such that the resultant structure is the most energy favorable arrangement. With this method, there is a possibility of formation of undesirable grain boundaries, which limits the spatial-phase coherence over a long distance.

The photolithography technique requires that light from a source passes through a photo mask having desired geometrical pattern, which will be incident on a photoresist. When this photoresist is developed, the pattern obtained is the result of photo mask geometry and the type of photoresist used (positive or negative). Another optical lithography technique, Interference Lithography, does not require a photo mask and is used to make periodic

structures. This method can be used to pattern larger area simultaneously and requires very short time. Due to the parallel processing of the large area, this method has very good spatial-phase coherence. The smallest period obtained is a function of the wavelength of light used. Like all optical lithography methods, this method also suffers diffraction limit imposed by the wavelength of the light. In this thesis, I will address this issue and will propose a methodology which will further push down the diffraction limit, to make sub wavelength periodic structures.

1.3 Thesis Structure:

In this thesis I present immersion interference lithography for sub wavelength periodic structures in the following sequence. Chapter 2 covers the concepts of interference lithography and the set-up design of Lloyd's mirror interferometer. It also includes the results obtained by using this set-up. Chapter 3 outlines the state of the art in the immersion lithography with some recent work in this field. The proposed method will be introduced in this chapter. I will also address the issues involved in using immersion lithography and their effect on the proposed methodology. In chapter 4, I will present the stack design for the samples used to perform these experiments. Results obtained using the proposed method will be presented and discussed. This chapter will be concluded with the comparison of results for mediums having different refractive indices.

Chapter 2 Interference Lithography

In this chapter, background information on interference of light will be provided. It will then be followed by the section explaining fabrication process used for interference lithography. The last section will cover the Lloyd's mirror interferometer.

2.1 The Principal of Interference of Light:

Light is a form of electromagnetic energy, described as an electromagnetic wave. The electromagnetic wave can be specified by two vectors, the electric field $\vec{E}$ and the magnetic field $\vec{H}$. For a light propagating through a source free, linear, isotropic and homogenous region, the electric and magnetic fields are related by the Maxwell's equations. The fields in these equations are functions of both position *r* and time *t*. More details on electromagnetic theory can be found in [12], [13], and [14].

$$\nabla\times\vec{\mathrm{E}}(\vec{\mathrm{r}},\mathrm{t}) = -\mu\frac{\partial\vec{\mathrm{H}}(\vec{\mathrm{r}},\mathrm{t})}{\partial\mathrm{t}} \tag{2.1}$$

$$\nabla\times\vec{\mathrm{H}}(\vec{\mathrm{r}},\mathrm{t}) = \varepsilon\frac{\partial\vec{\mathrm{E}}(\vec{\mathrm{r}},\mathrm{t})}{\partial\mathrm{t}} \tag{2.2}$$

$$\nabla\cdot\vec{\mathrm{E}}(\vec{\mathrm{r}},\mathrm{t}) = 0 \tag{2.3}$$

$$\nabla\cdot\vec{\mathrm{H}}(\vec{\mathrm{r}},\mathrm{t}) = 0 \tag{2.4}$$

Where, μ and ε are the permeability and permittivity of the medium through which the light propagates.

The electric and magnetic fields in the two curl equations can be separated to form a wave equation;

$$\nabla^2\vec{E} - \frac{1}{c^2}\frac{\partial^2\vec{E}}{\partial t^2} = 0 \tag{2.5}$$

$$\nabla^2\vec{H} - \frac{1}{c^2}\frac{\partial^2\vec{H}}{\partial t^2} = 0 \tag{2.6}$$

Here, *c* is the speed of light.

Maxwell's equations are linear differential equations and the solution to this set of equations is given by;

$$\Psi = Ae^{j(\omega t - \vec{k}.\vec{r})} \tag{2.7}$$

The electric and magnetic fields can be found using complex function formulation;

$$\vec{E}(\vec{r},t) = E_{\circ}e^{(-j(\vec{k}.\vec{r}-\omega t)} \tag{2.8}$$

$$\vec{H}(\vec{r},t) = H_{\circ}e^{(-j(\vec{k}.\vec{r}-\omega t)}$$

Where, E_0 and H_0 are the magnitudes of electric and magnetic field respectively, ω is the angular velocity of the wave, k is the wave vector and its magnitude in terms of wavelength λ, is given by;

$$| \vec{k} | = k = \frac{2\pi}{\lambda} \tag{2.9}$$

In case of interference lithography, we are interested in knowing the exposure dose required to get the desired pattern in the photoresist. This is the amount of energy received by the photoresist per unit area per unit time. This quantity is known as optical intensity or irradiance and is given by following equation;

$$I = \varepsilon \upsilon < \vec{E}^2 >_T \tag{2.10}$$

Where, υ is the velocity of light through which the light travels and the pointy bracket indicates the time averaged quantity. Here, we will be considering the electric field only as it is more effective at exerting forces and doing work on charges than the magnetic field.

By dropping the proportionality constants, we get;

$$I \approx < \vec{E}^2 >_T = < \vec{E} \cdot \vec{E}^* >_T \tag{2.11}$$

We are interested in the phenomenon in which two coherent plane waves are added together such that the resultant wave has either greater or lower amplitude. This is known as interference. Consider two waves of the form;

$$\vec{E}_1(\vec{r},t) = A_1 e^{(-j(\vec{k}_1.\vec{r}-\omega t)} \tag{2.12}$$

$$\vec{E}_2(\vec{r},t) = A_2 e^{(-j(\vec{k}_2.\vec{r}-\omega t+\Delta\phi)} \tag{2.13}$$

These two waves interfere with each other to form an interference pattern.

$$I = \left|\vec{E}_1 + \vec{E}_2\right|^2$$

$$I = (\vec{E}_1 + \vec{E}_2)(\vec{E}_1^* + \vec{E}_2^*)$$

$$I = I_1 + I_2 + [(\vec{E}_1 \cdot \vec{E}_2^*) + (\vec{E}_1^* \cdot \vec{E}_2)]$$

$$I = I_1 + I_2 + 2(\vec{E}_1 \cdot \vec{E}_2)\cos[(\vec{k}_1 - \vec{k}_2) \cdot \vec{r} + \Delta\phi] \tag{2.14}$$

It is easier to measure intensity than measuring electric field. So, we will use magnitudes of electric field in equation (2.15).

$$I = I_1 + I_2 + 2\sqrt{I_1 I_2}\cos\delta \tag{2.15}$$

Where, δ is the phase difference arising from combined path length and initial phase-angle difference between two waves represented by equations (2.12) and (2.13). Equation (2.14) gives the total irradiance due to two interfering waves.

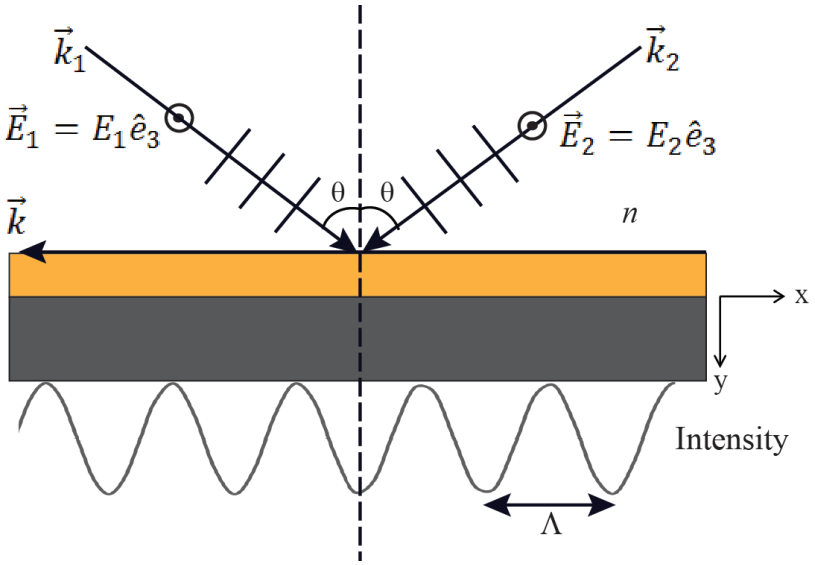

Figure 2-1: Periodicity of interference pattern

The two plane waves represented by equation (2.12) and (2.13) interfere with each other to give a sinusoidal intensity pattern. The maxima and minima of this sinusoidal intensity pattern are known as fringes. We are interested in finding the periodicity of these fringes as these will define the period of the structure that we get using interference lithography. The fringe vector is given by;

$$\vec{k} = \vec{k}_1 - \vec{k}_2 = k_x\hat{e}_1 + k_y\hat{e}_2 + k_z\hat{e}_3 \tag{2.16}$$

Assume the spatial vector $\vec{r}$ is parallel to the fringe vector $\vec{k}$, also $\vec{r}$ and $\vec{k}$ are along *x*-axis. The spatial phase then can be written as a product of magnitude of fringe vector and the spatial position.

$$\delta = |\vec{k}|r$$

The spatial periodicity is then given by;

$$\Lambda = \frac{2\pi}{\vec{k}} \tag{2.17}$$

For two beams drawn from a single monochromatic source of light, magnitude of wave vector is same i.e. $|\vec{k}_1| = |\vec{k}_2|$. The individual vector components along unit axis are related as; $k_{2e_1} = -k_{1e_1}$, $k_{1e_2} = k_{2e_2}$, $k_{1e_3} = k_{2e_3}$. Substituting this equation 2.16, we get;

$$\vec{k} = 2k_{2e_2}\hat{e}_2 \tag{2.18}$$

Using this result and with equations (2.9) and (2.17), we get the following relation for periodicity of fringes;

$$\Lambda = \frac{\lambda|k_2|}{2k_{2e_2}} \tag{2.19}$$

From figure 2-1, we can define the relationship between angle of incidence one of the wave vector.

$$sin\theta = \frac{k_{2e_2}}{|\vec{k}_2|}$$

So the periodicity of the two interfering beams is given by equation (2.20) and this identity is valid only when the only when the angle bisector of two interfering beams is normal to the direction of fringe period.

$$\Lambda = \frac{\lambda}{2sin\theta} \tag{2.20}$$

2.2 Fabrication using Interference Lithography:

The interference lithography uses the principal of interference of two coherent plane waves to form an in intensity pattern. As shown in figure 2.2, two rays of light having same wavelength, are incident on the substrate at an angle θ. When these two rays of light interfere with each other, they create an intensity pattern as shown. This intensity is then received by the photoresist. When this photoresist is developed, the resulting structure looks as in figure 2-3, which has 1D grating on it.

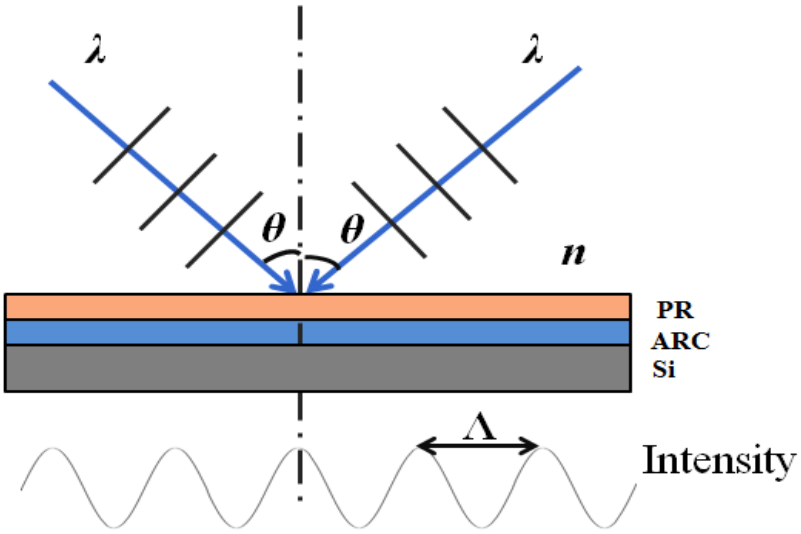

Figure 2-2: Interference Lithography

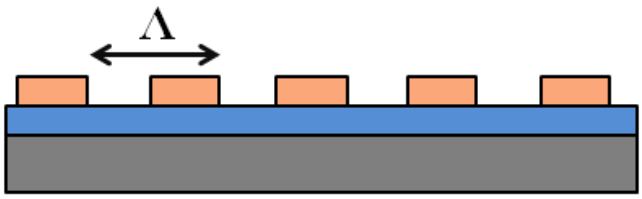

Figure 2-3: Gratings after developing the photoresist

Interference lithography is suitable for making periodic structure and it cannot be used to make any arbitrary structures on the substrate [17]. Interference lithography can attain high spatial-phase coherence, which is difficult with other methods. Another advantage of interference lithography is that, it can produce structures with very high resolution. The period (Λ) of the structure produced by interference lithography is given by,

$$\Lambda = \frac{\lambda}{2nsin(\theta)} \tag{2.21}$$

Where, λ is the wavelength of the light, n is the refractive index of the medium through which light travels and θ is the angle at which the light is incident on the substrate. By changing any of these three parameters, we can vary the period of the structure.

2.3 Lloyd's Mirror Interferometer:

As a part of my master's research, I built a Lloyd's mirror interference lithography setup. Lloyd's mirror interferometer uses the principal of interference lithography with one modification in the set-up. Lloyd's mirror uses only a single source of light to create the interference pattern. As shown in figure 2-4, the mirror, which is at 90°, acts as a second source of light, and the light reflected from the mirror interferes with the light coming directly on the substrate to form the intensity pattern. Figure 2-4 shows the schematic of the Lloyd's mirror interferometer;

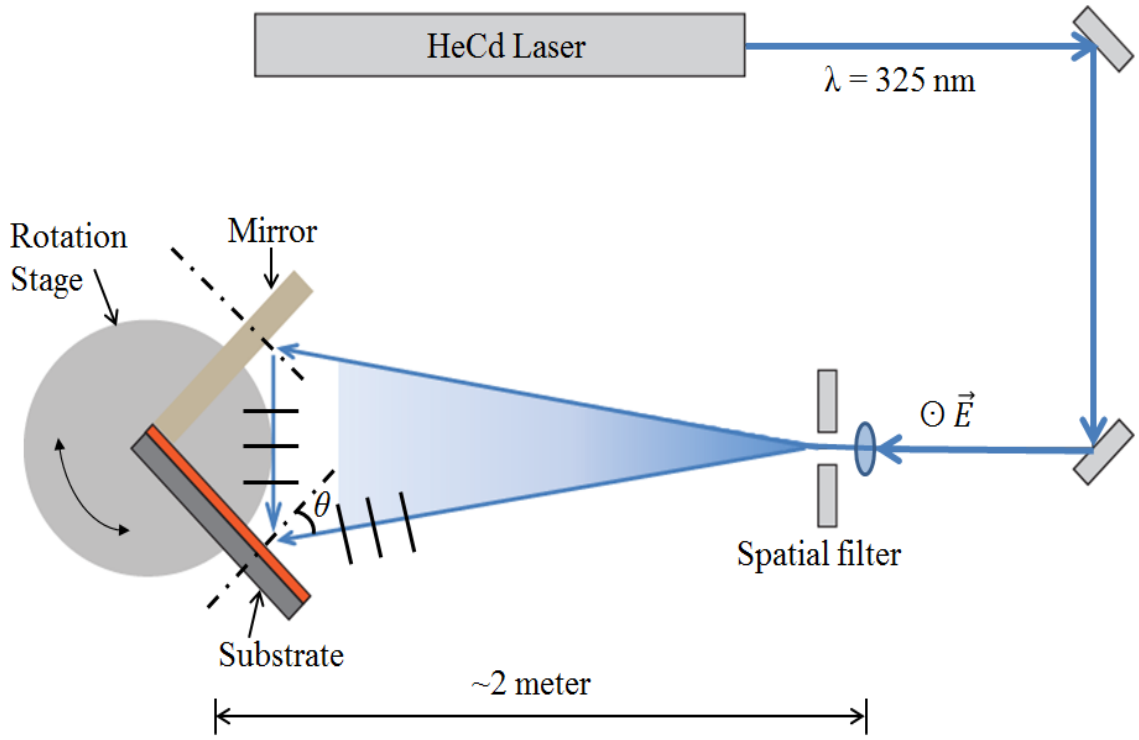

Figure 2-4: Lloyd's Mirror Interferometer

The interferometer consists of wafer chuck which uses vacuum to hold the wafer, a mirror and a rotary stage. The rotary stage, allows to change the angle at which light is incident on the substrate, thereby changing the period of the structure produced. The relation between angle and period is given by equation (2.21). The set-up uses a HeCd laser with a wavelength of 325 nm. The mirrors between laser and spatial filter are arranged in such a way that, the polarization incident on the substrate is TE i.e. electric field is perpendicular to incident plane. The spatial filter is used to provide a clean Gaussian beam by removing high frequency noise and the beam coming out of it is a spherical wave. The distance between spatial filter and the wafer chuck is approximately 2 meters. The spherical wave expands in

diameter over this path, which helps to create a more uniform intensity distribution over the exposed area. The intensity of the wave decreases as the wave expands, but it can be compensated by increasing the exposure time. Also, the increase in the radius of phase front means that the beam closely approximates to a plane-wave front after 2 meter distance. Longer beam expansion ensures that the exposed grating will have a more linear spatial phase and more uniform line width [15], and [16].

2.4 Lloyd's Mirror Chuck Design:

Principal of Lloyd's mirror interferometer is based on interference of two beams, one of these two beams is the light reflected from a mirror which is at exactly 90° to the substrate. Therefore, it is critical that the substrate and mirror should remain perpendicular to each other, during exposure. Figure 2-5 shows the design of the substrate holder. The holder has an array of interconnected holes ($\text{diameter} = 0.06\,\text{inch}$). The substrate will be placed on this array and will be held against the holder by making use of vacuum. Use of vacuum simplifies the loading and unloading of substrate and also ensures that the substrate is perfectly flat. The holes on the side walls of wafer holder are drilled to interconnect all holes, which will be plugged before using the system for exposure. The bigger interconnected holes ($\text{diameter} = 0.1\,\text{inch}$) and the groove are used to hold the mirror mount holder against wafer holder, using vacuum. The smaller and bigger holes have separate vacuum lines, located at the back side of the wafer holder.

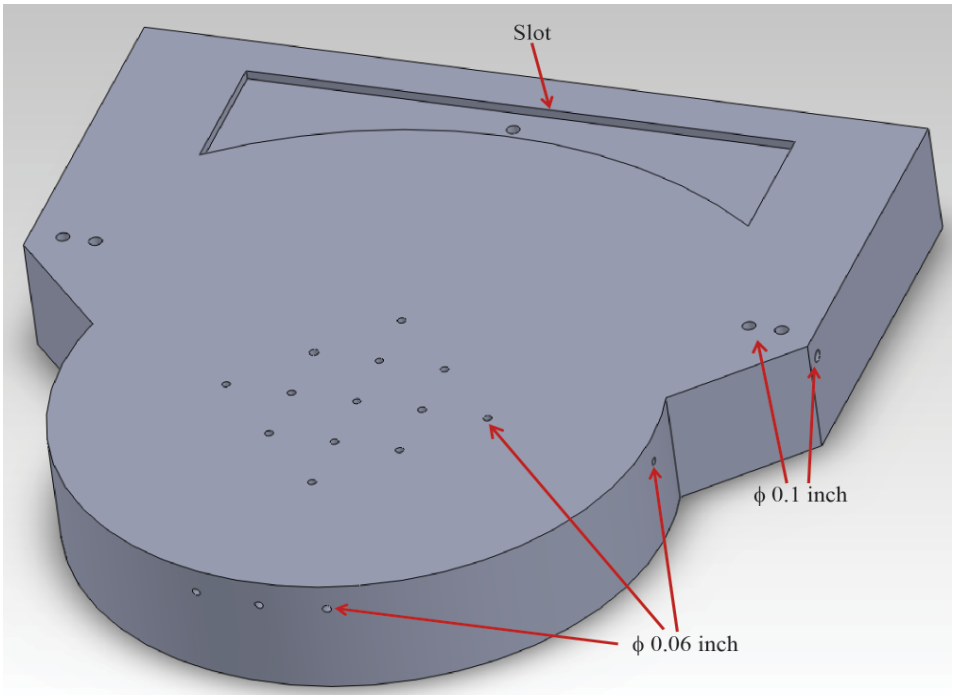

Figure 2-5: SolidWorks model of wafer holder

Figure 2-5 shows the design of mirror mount holder, which will ensure that the mirror is at exactly 90̊ to the substrate. The mirror mount will be connected to mirror mount holder. A semi-circular step is provided on the mirror mount holder, to ensure that the mirror will remain perpendicular to the substrate, while using a whole 4 inch wafer. A groove on the mirror mount holder aligns with the slot on the wafer holder, with slot completely enveloped by the groove. As metal to metal contact is not good, so when the vacuum is turned on, there is possibility of air leakage between two metal surfaces. To avoid this, a rubber ring will be placed in the groove. This rubber ring will get squeezed when the vacuum is turned on. This will avoid air leakage and both wafer holder and mirror mount holder will be firmly held against each other.

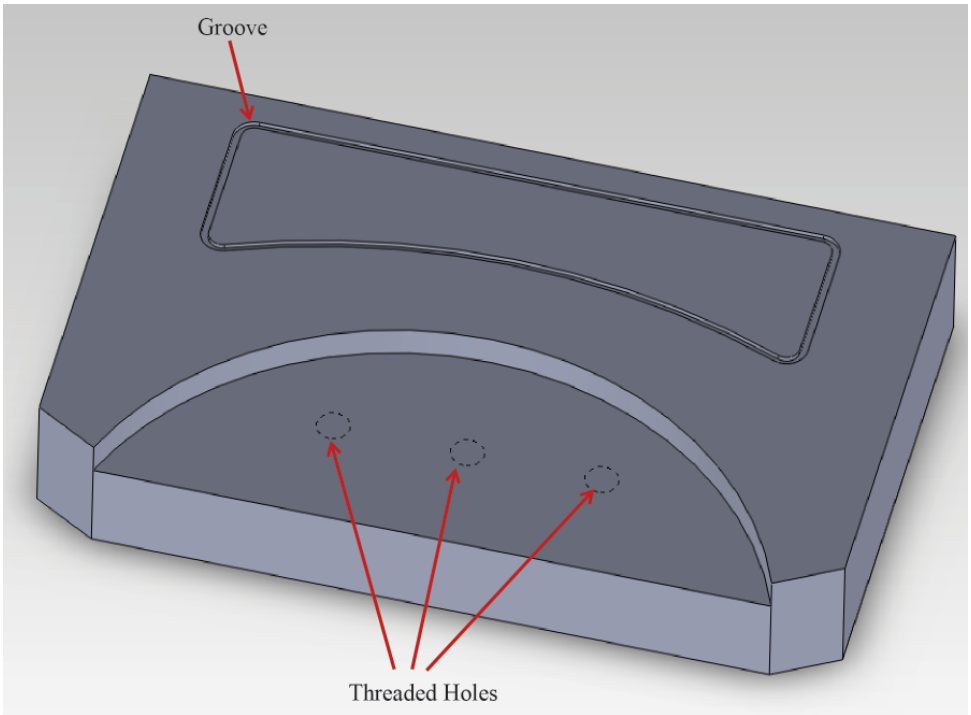

Figure 2-6: SolidWorks model of mirror mount holder

Figure 2.7 shows the actual setup of the vacuum chuck used in Lloyd's mirror interferometer. The vacuum chuck is mounted on a rotary stage, which is used to adjust the system to the desired angle of incidence. The arrangement is made such that, the axis of rotation of the rotary stage and the line of intersection of mirror and wafer coincide with each other. This arrangement ensures that, the chuck and the pin hole are always aligned and do not need any adjustment of the pinhole, when the angle of incidence is changed. During exposure, the wafer is held in place by using vacuum. Also, the arrangement of mirror and wafer is such that they are always normal to each other during the exposure.

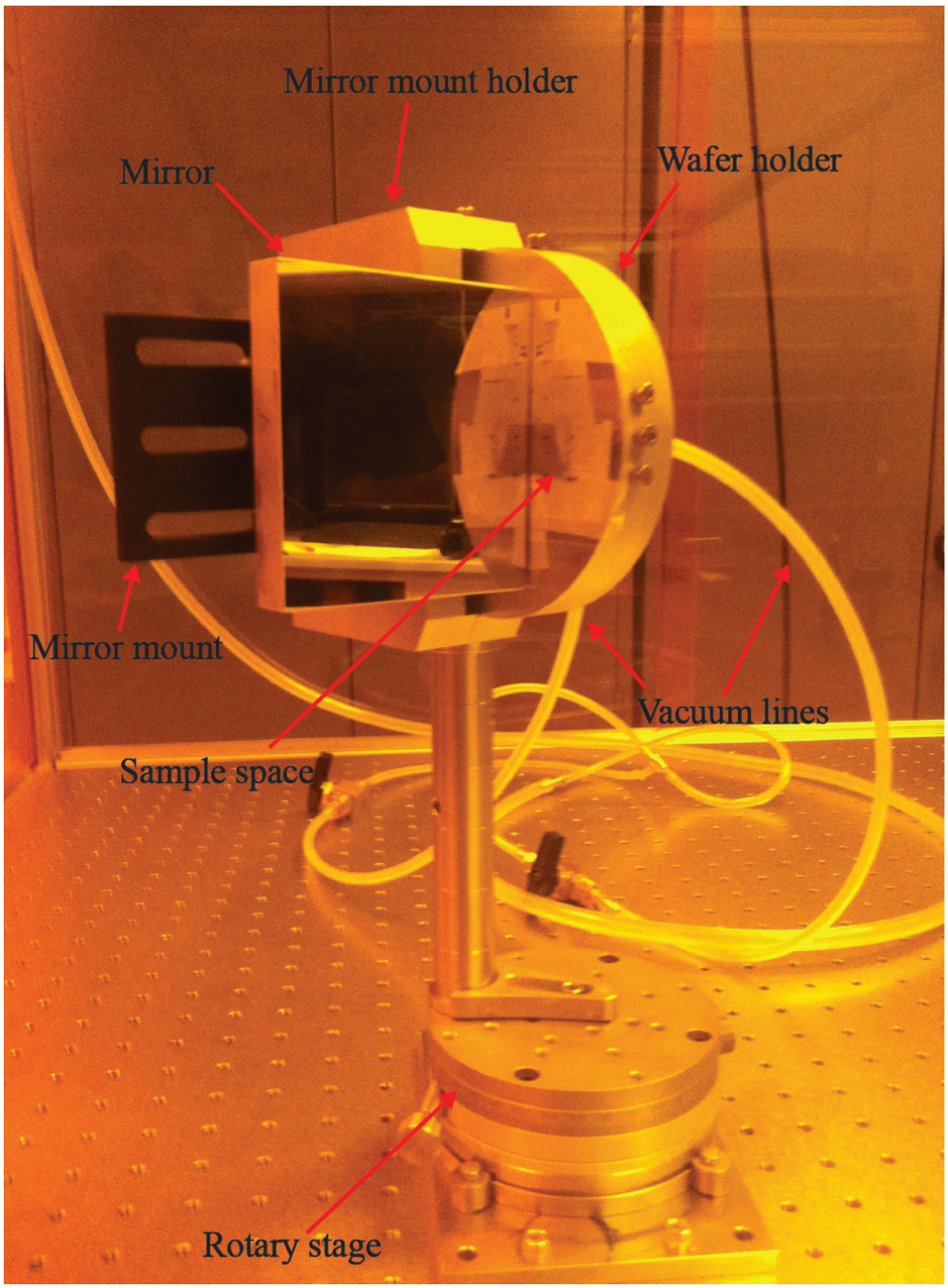

Figure 2-7: Lloyd's Mirror Interferometer setup

2.5 Stack Design and Experimental Results for Lloyd's Mirror Interferometer:

This section will cover the stack design used for fabricating periodic structures using Lloyd's mirror interferometer. Here, the stack design details are provided for periodicity of 200 nm and 500 nm. It is possible to make a structure having any period with this range, by changing the angle of incidence of light.

The thickness of ARC needs to be optimized to reduce the reflection at the photoresist – ARC interface, and this can be done by examining light reflection in the thin films [18]. More details on the necessity of using ARC layer in the stack design are provided in section 4-1. The air and silicon substrate are assumed to be semi-infinite due to relatively large dimensions compared to photoresist and ARC layer. Here, a positive photoresist is used as it gives higher resolution and high aspect ratio, when the reflection from ARC layer is low. The parameters used in stack design are listed in Table 2-1.

Table 2-1: Material characteristics for ARC thickness optimization

Layer #	Medium	Thickness	Refractive Index @ 325 nm
1	Air	semi-infinite	1
2	Photoresist (Sumitomo PFI-88)	200 nm & 500nm	1.79-0.02i
3	ARC (ARC-i-CON-7)	$\mathbf{t_{arc}}$	1.445-0.3402i
4	Silicon substrate	semi-infinite	4.68-2.03i

Using these parameters, the optimum thicknesses for 200 nm and 500 nm are 109.4 nm and 97.4 nm respectively.

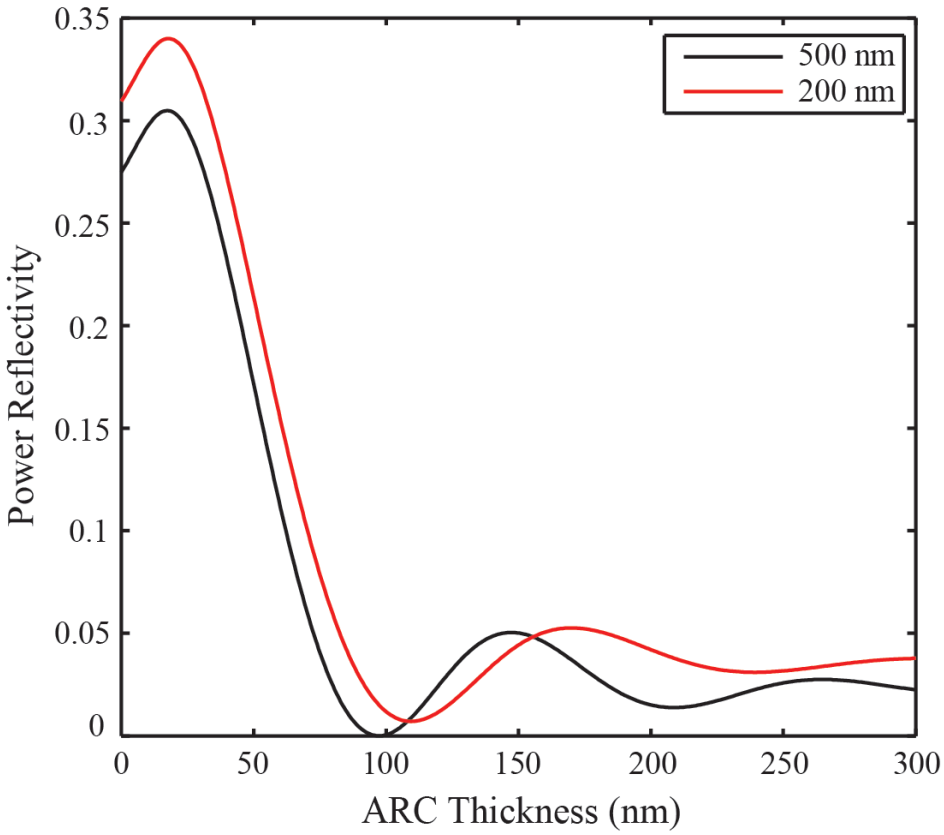

Figure 2-8: Reflectivity vs. ARC thickness

Figure 2-8 plots the power reflected by the ARC layer at photoresist-ARC interface as a function of ARC thickness. It is necessary to reduce the reflection from the ARC layer, to get a better contrast of the structure. If the reflection is higher than 1%, the fabricated structure will not have straight walls and the structure profile will be poor. For 500 nm period, when using the materials specified in table 2-1, the reflected power is almost zero and

for 200 nm period, the minima is at 0.7%. Results obtained using these stack designs are shown in figure 2-9.

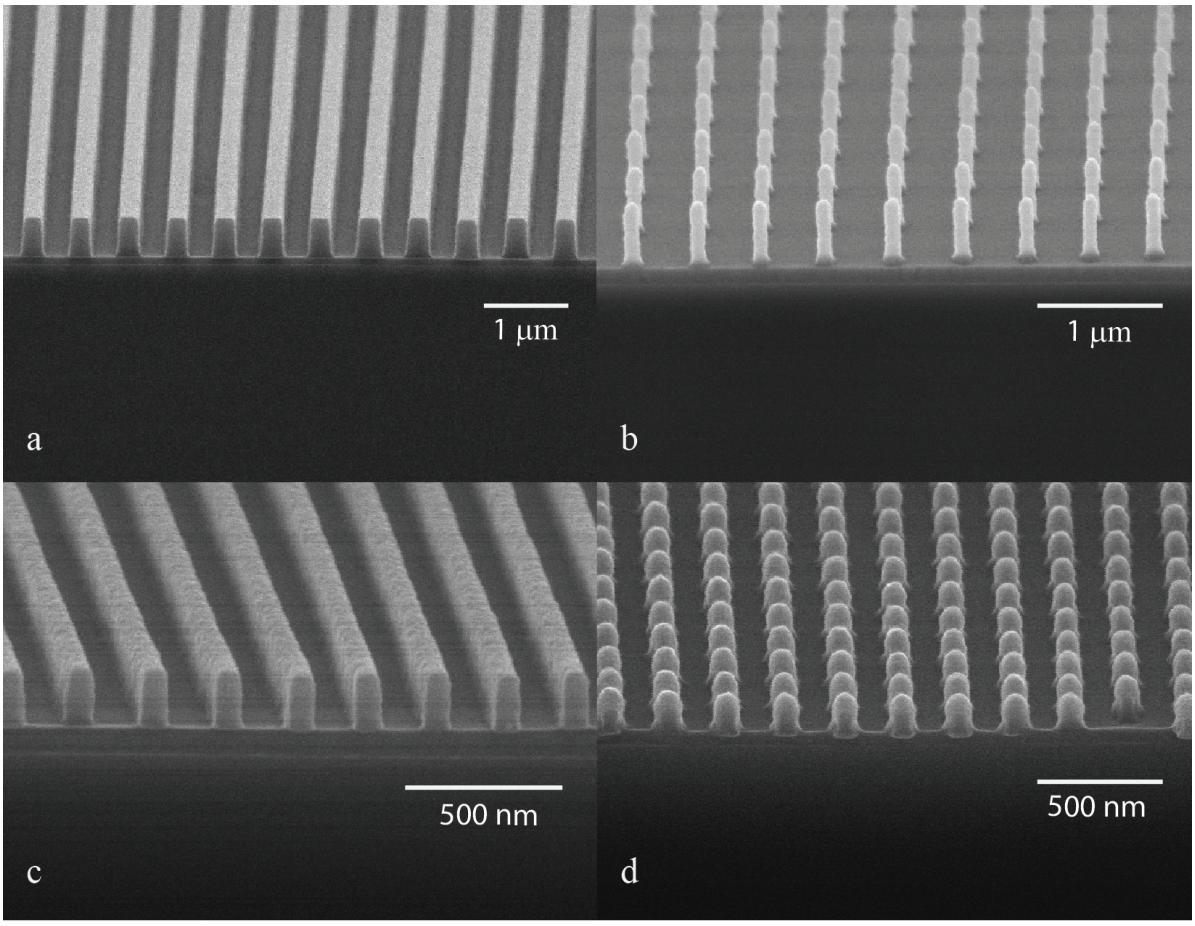

Figure 2-9: Interference lithography results in air
(a) 1D 500 nm (b) 2D 500 nm (c) 1D 200 nm (d) 2D 200 nm

For both 1D and 2D structures, it is possible to control the line width by controlling the exposure dose at which the sample is exposed. In figure (a), the line width is almost half of the total period, whereas in figure (b), the line width is very small due to longer exposure. Figure (c) and (d) have fairly similar line width.

Chapter 3 Immersion Interference Lithography (IIL)

In this chapter, a brief overview of the current state of art in immersion lithography will be given. It will then be followed by the setup design for the proposed method, for immersion interference lithography, which combines immersion lithography with the Lloyd's mirror interferometer. This chapter will also provide a background on absorption of light by immersion fluid, followed by the transmittance calculations for Cargille Fluid 50350. The chapter will then be concluded with contrast analysis of the structures, fabricated by the proposed method.

We saw that, using Lloyd's mirror it is possible to expose a fairly large area of the substrate. For a laser of 325 nm wavelength, it is possible to get a period of the structure in the range of 200 nm - 500 nm. This is achieved by rotating the stage, i.e. by changing the angle at which the beam is incident on the substrate. The smallest period that can be produced using this system is given by;

$$\Lambda \sim \frac{\lambda}{2n}$$

From equation (2.22), it is clear that, if we want to get a smaller period, we will have to use a laser with smaller wavelength. Though this seems to be a very simple solution, such lasers are very expensive and the increase the cost of producing the periodic structure. The other way is to increase refractive index of the medium through which light propagates before it is incident on the substrate. This is usually achieved by passing the light through

high refractive index fluid. In the next section, we will briefly discuss few of the techniques that are currently available. Also, a new method for Immersion Interference Lithography will be introduced.

3.1 Immersion Lithography:

The resolution of the fabricated structure can be enhanced either by reducing the wavelength of the laser used or by increasing the refractive index of the medium through which light travels. It is expensive to use small wavelength lasers, so we will focus on getting higher resolution by using high refractive index medium.

Immersion Lithography has caught IC manufacturer's attention due to its ability to fabricate high resolution microelectronic devices, by utilizing the high refractive index of immersion fluid. The fluids used in this method must be fairly optically transparent i.e. it should have very low absorption at desired wavelength of the light. Immersion lithography techniques for 193 nm wavelength laser are well established [21]. In semiconductor industry, 193 nm immersion scanners are used to manufacture integrated circuits with higher resolution. These scanners use highly purified water as immersion fluid, which has refractive index of 1.44 for 193 nm wavelength. This method uses a mask to fabricate structures.

Figure 3-1 shows schematic of the immersion lithography [22, 23], in which, a high refractive index fluid is placed between the lens and the substrate. The light exiting the lens travels through the immersion fluid before it enters the photoresist. When light enters in the high refractive index medium, its wavelength gets reduced, proportional to the refractive index of the fluid ($\lambda = \frac{\lambda_{vac}}{n}$).

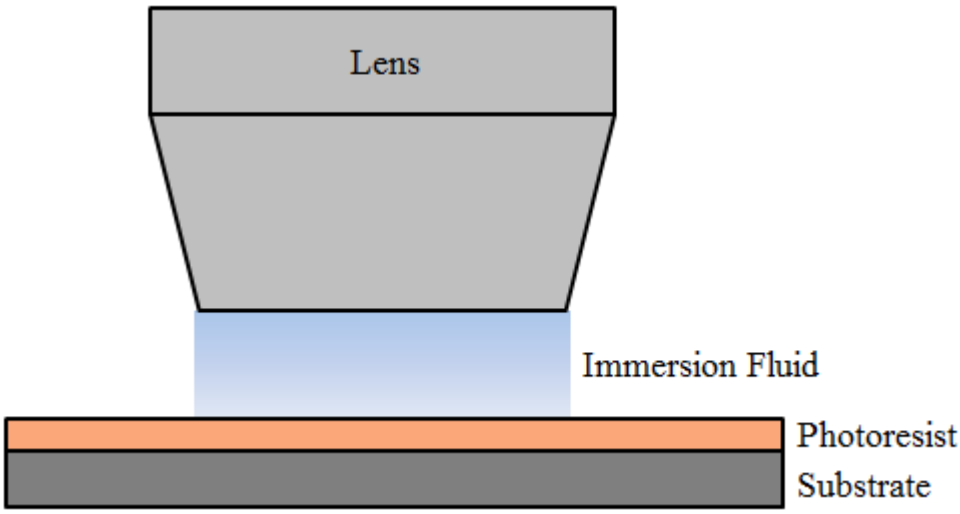

Figure 3-1: Schematic of Immersion Lithography using Scanner

Recent efforts have been focused on making periodic structures using immersion lithography, which can be achieved by combining immersion lithography technique with the Lloyd's mirror interferometer. De Boor et. al. [19] uses a sapphire prism, with one face polished to act as a mirror and the other face rests on the substrate. The immersion fluid is spin coated on the substrate and the prism is pressed against it to ensure conformal contact. With this method, structure with period smaller than 100 nm has been fabricated using a laser of 244 nm wavelength. Another research group [20] uses two beam interference technique to make the periodic structure. Structure with periodicity of 44nm has been fabricated using 157 nm wavelength laser. This method also spin casts the immersion fluid on photoresist.

3.2 Motivation:

Though the methods discussed earlier have been successful in fabricating smaller structures using the immersion fluids with higher refractive index, there are some operational difficulties which need to be addressed to simplify the process. Methods in [19, 20] need some mechanism to maintain a liquid layer between lens/prism and the substrate, as it is very difficult to maintain constant thickness of liquid at all places. There is a possibility of formation of air pockets, trapped between prism and the wafer due to the poor contact. In such a case, it is difficult to get a good structure over large area. These methods use a sapphire prism, which needs to be machined very precisely and the prism can get damaged during its use. Though the refractive index of sapphire prism is very high, the period of the structure is dependent only on the refractive index of the immersion fluid used. Again, with these systems, it is not be possible to fabricate structures with different periodicity, without changing incident angle on the solid prism. This may require a new prism if we want to change the period by larger amount. In [24, 25] multilevel interference lithography has been successfully used to make the structures with 50 nm period. But this method requires multiple exposures to fabricate smaller period and also requires very precise alignment of the setup. The 193 nm scanner uses an expensive mask to fabricate periodic structures and there is always a possibility of spilling of immersion fluid, during exposure, which might contaminate the system. To address these issues, a new system is proposed, which will be introduced in next section.

3.3 IIL System Design:

IIL is designed to address the shortcomings of the available methods. We wanted the system to be flexible, so that we can produce sub wavelength structures with a large period range using the same system. We also wanted to simplify the system by completely eliminating the mechanism needed to maintain the continuous liquid contact between lens and substrate. We make use of gravity to maintain continuous contact between the substrate and the immersion fluid. Unlike the available methods which use solid-liquid immersion, this method uses only liquid and eliminates machining cost. In this proposed method, we get a better contact between the substrate and the immersion fluid and there is no possibility of formation of air gaps. So, we can fabricate the structure over a large area without any defects. In available methods, the periodicity is changed by changing the angle on the sapphire prism, which is quite expensive and time consuming. In the proposed method, we can get any desired periodicity of the structure, over a range, simply by adjusting the container holding the immersion fluid to the desired angle. This attribute makes the system very flexible and significantly reduces the time required for arranging the setup. The new method combines the principles of immersion lithography with the Lloyd's mirror interferometer. This method is very compact and requires minor adjustment to get structures with different periodicity. Following figure shows the schematic of the proposed set-up;

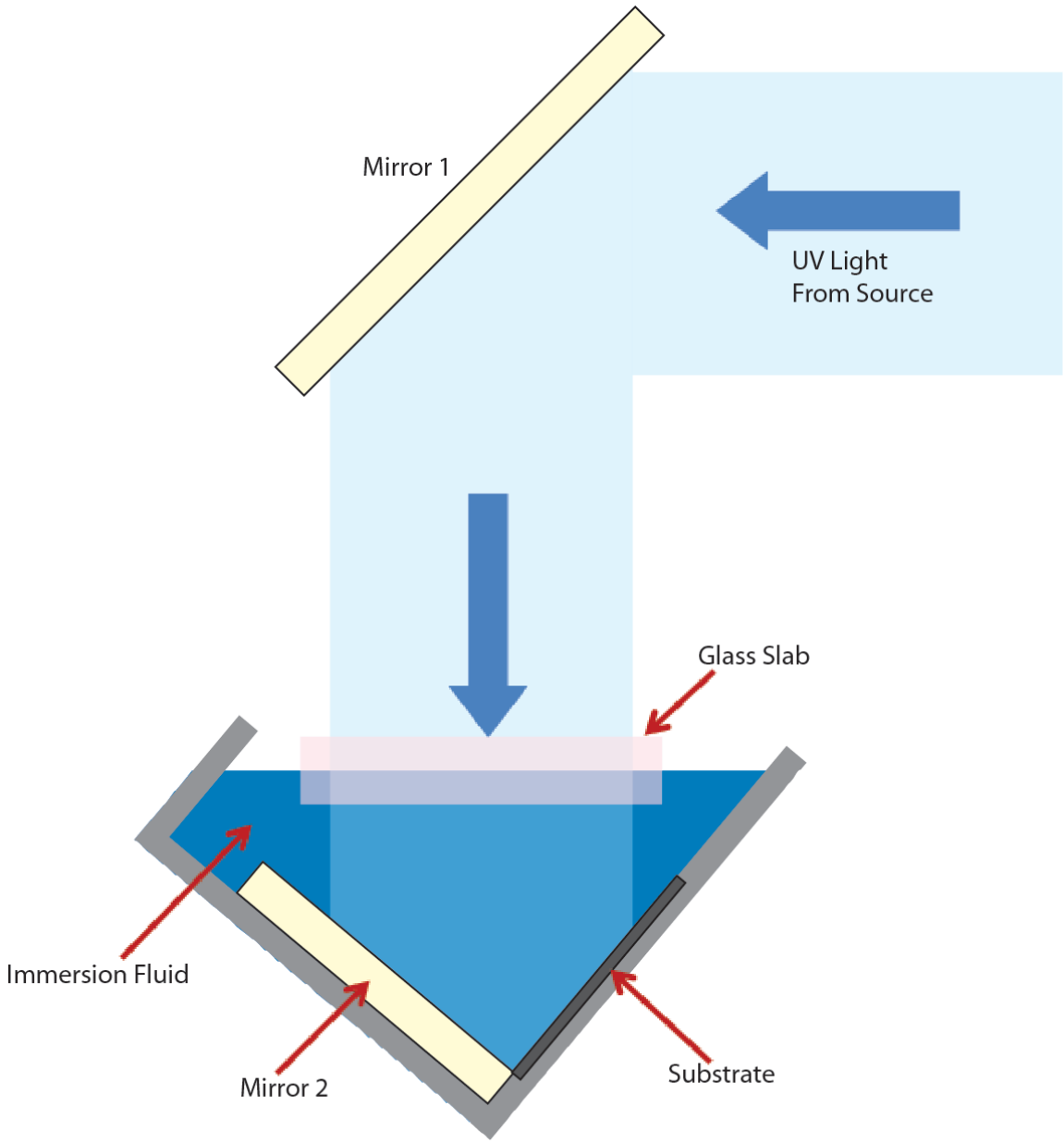

Figure 3-2: Schematic of Immersion Interference Lithography set-up

In Lloyd's Mirror Interferometer, the UV light travels through air which has refractive index 1. In case of IIL, we can use the immersion fluid with higher refractive index

to get smaller period. Figure 3-2 shows the proposed immersion interference setup in which the Lloyd's mirror interferometer is immersed in the immersion fluid. The ultra-violet light from the laser is incident on Mirror-1 inclined at 45°. The reflected light from the Mirror-1 falls on the container which is filled with immersion fluid. Selection of the immersion fluid is based on the desired period of the structure. Mirror-2 is mounted on one face of the container and the other face has a groove for mounting the substrate. Mirror-2 and the substrate will always be at 90° to each other, thereby replicating the Lloyd's Mirror Interferometer. In figure 3-2, we can see that a glass slab is used and is partially immersed in the immersion fluid. The UV light coming through the air is normally incident on this glass slab and then it enters the immersion fluid. The purpose of this slab is to ensure that, any ripples caused on the surface of the immersion fluid will not hinder the light from air entering at a normal angle in the immersion fluid. In the absence of this slab, the ripples generated on the fluid surface might cause refraction of the light, while entering from air to immersion fluid.

The light passing through immersion fluid falls on both Mirror-2 and the substrate. The light from Mirror-2 is reflected again and falls on the substrate creating an interference pattern on the substrate as shown in figure 3-3. In figure 3-3, θ is the angle of incidence for light and it is adjusted by adjusting the angle of the container. Λ is the period of the structure that we get and it depends on refractive index of the immersion fluid and angle of the container (θ).

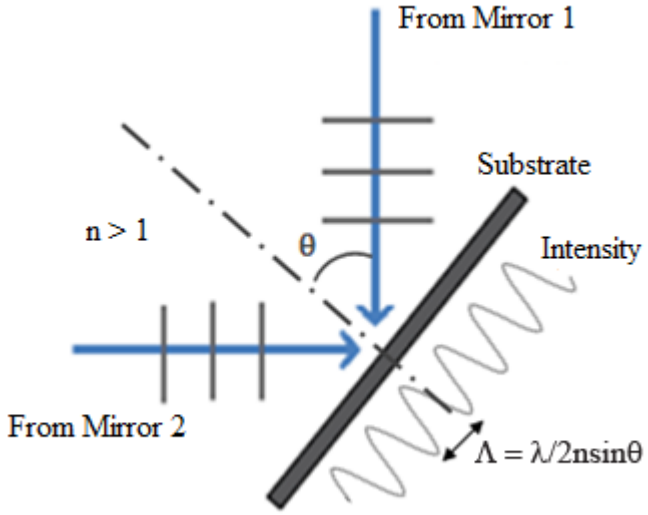

Figure 3-3: Schematic of interference mechanism for IIL

Figure 3-4 shows the SolidWorks model of the container used to carry out these experiments. This container can rotated about the axis shown in the figure, so as to change the angle at which light is incident on the substrate. By rotating the container about this axis, various incidents angles in the range of 20° to 75° can easily be obtained. Figure 3-5 shows the cross-section of the container, with the positions of the mirror and the substrate marked.

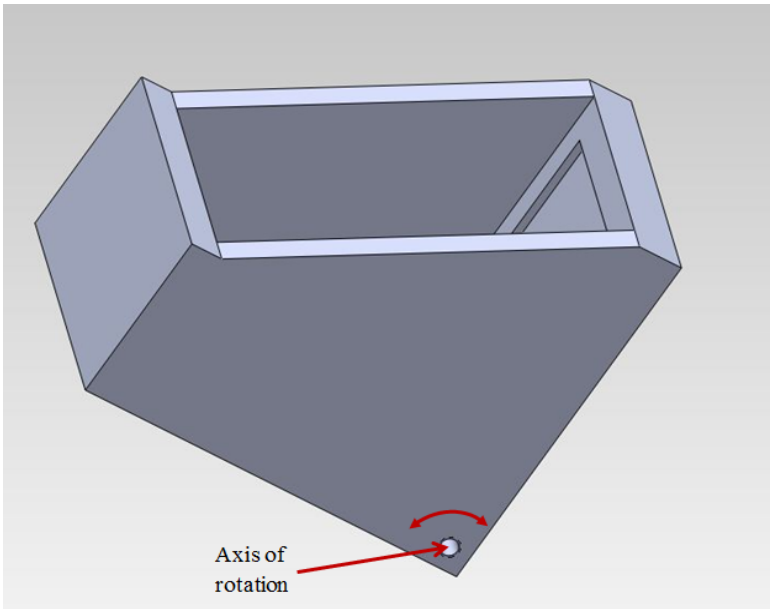

Figure 3-4: SolidWorks model of acrylic container with axis of rotation

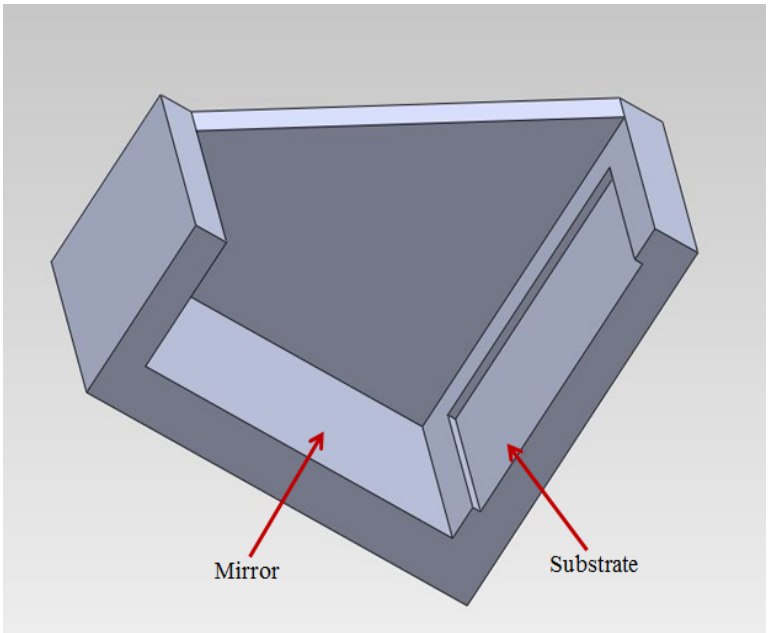

Figure 3-5: Cross-sectional view of the container with mirror and substrate position marked

Figure 3-6 shows the actual setup used to carry out experiments. The container and the mirror mount are connected to a single optical post, to ensure that the whole setup will experience same disturbance, if any, due to external vibrations. The container has 6 degrees of freedom and can be adjusted to any desired angle and height. The mirror mount is always kept at the same position to provide process stability. The glass slab is glued to a black connecting tube, which is connected vertically to the mirror mount. The container is made from acrylic as it is lighter in weight, absorbs UV light and its pieces are easier to glue together.

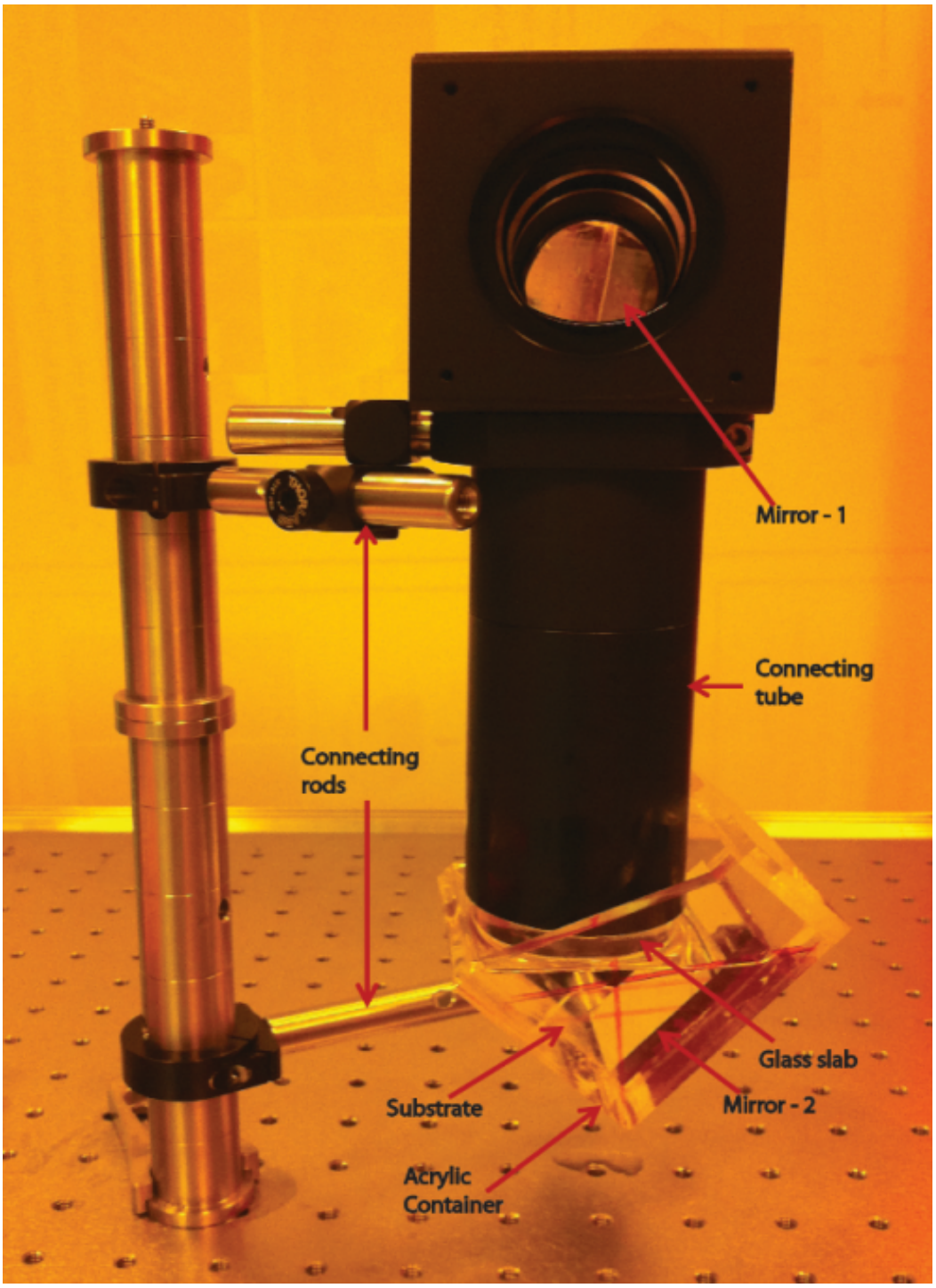

Figure 3-6: Actual set-up used for Immersion Interference Lithography

3.4 Absorption in Immersion Fluid:

Though immersion fluids provide higher refractive index, they are absorbing at the smaller wavelengths, thereby limiting the use of immersion lithography. The absorption phenomenon is characterized by the absorption/attenuation coefficient of the medium. Smaller absorption coefficient means the medium is relatively transparent and vice versa. The absorption coefficient is related to wavelength of light and refractive index of medium by following formula;

$$\alpha = \frac{2\pi\kappa}{\lambda_0} \tag{3.1}$$

α – Absorption coefficient

κ – Imaginary part of the refractive index of the medium

λ_0 – Wavelength of the light in vacuum

The intensity of the light reaching to the substrate is important as it determines the exposure time required to get the pattern. We consider the amount of light transmitted through the immersion fluid to calculate this exposure time. The light transmitted through the immersion fluid is related to the absorption coefficient and the thickness of the fluid slab through the following equation [12];

$$Transmittance\ (T) = \frac{I'}{I} = e^{-\alpha y} \tag{3.2}$$

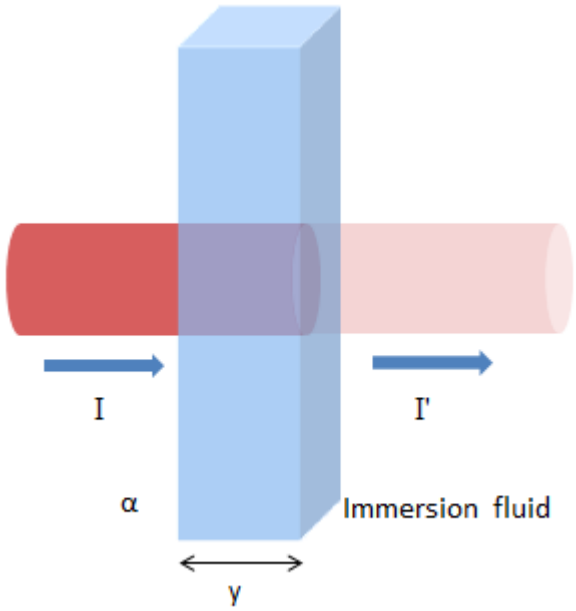

Figure 3-7: Schematic of absorbance phenomenon

In figure 3-7, the light of intensity (I) is incident from the left side of the liquid slab. When the light passes through the slab, some of the light gets absorbed by the liquid and its intensity decreases. The intensity of the transmitted light (I') depends on the absorption coefficient of the immersion fluid and thickness of the liquid layer (y).

We have used two immersion fluids; DI water and Cargille Fluid 50350. The refractive index of DI water is 1.33 and it does not absorb 325nm wavelength, thus giving the same intensity output as in air. But the Cargille Fluid which has refractive index of 1.5057@ 325, absorbs UV light when the liquid layer is thicker than 1cm. For the set-up proposed in this thesis, the liquid layer thickness varies in the range of 4-5cm depending on the angle at which the container is fixed.

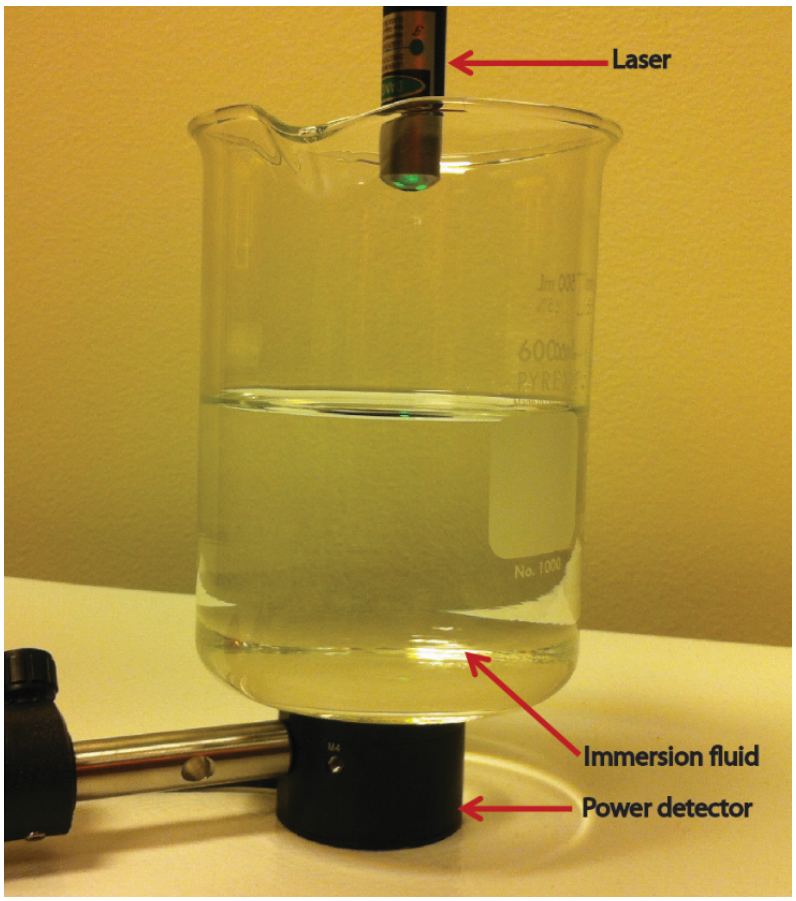

Figure 3-8: Transmittance measurement set-up

The figure 3.8 shows the arrangement used to measure the transmittance of the UV laser through immersion fluid. Actual readings are obtained for UV ($\lambda = 325nm$) laser instead of a green laser as shown above. Measurements are carried out at different thicknesses of liquid layer and the corresponding values of intensity are recorded. The light absorbed by the glass container is also considered for these calculations. The absorption coefficient of the Cargille Fluid 50350 is calculated, using equation (3.2), by taking few measurements of intensity of light before and after passing through the liquid layer. The value we got for

absorption coefficient is 0.0606 and is the average of all the experiments. Following table summarizes the experiments for calculating the absorption coefficient of the Cargille Fluid 50350;

Table 3-1: Experimental data for absorption coefficient

I ($\mu W/cm^2$)	I' ($\mu W/cm^2$)	Transmittance (%)	y (cm)	α
70	65.0	92.9	1.2	0.0614
70	58.5	83.6	3.2	0.0600
70	55.2	78.9	4	0.0592
70	50.1	71.6	5.4	0.0619

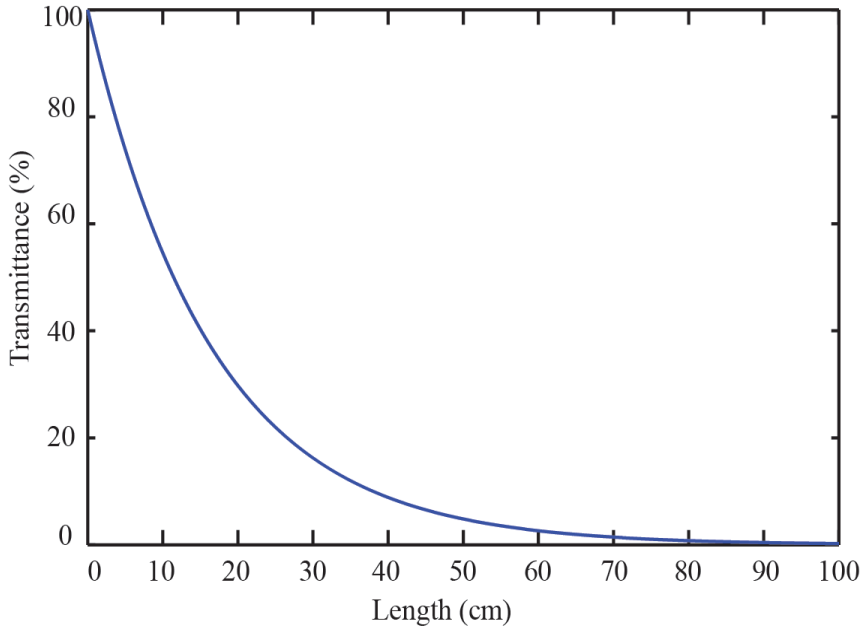

Figure 3-9: Transmittance vs. Path Length for Cargille Fluid 50350

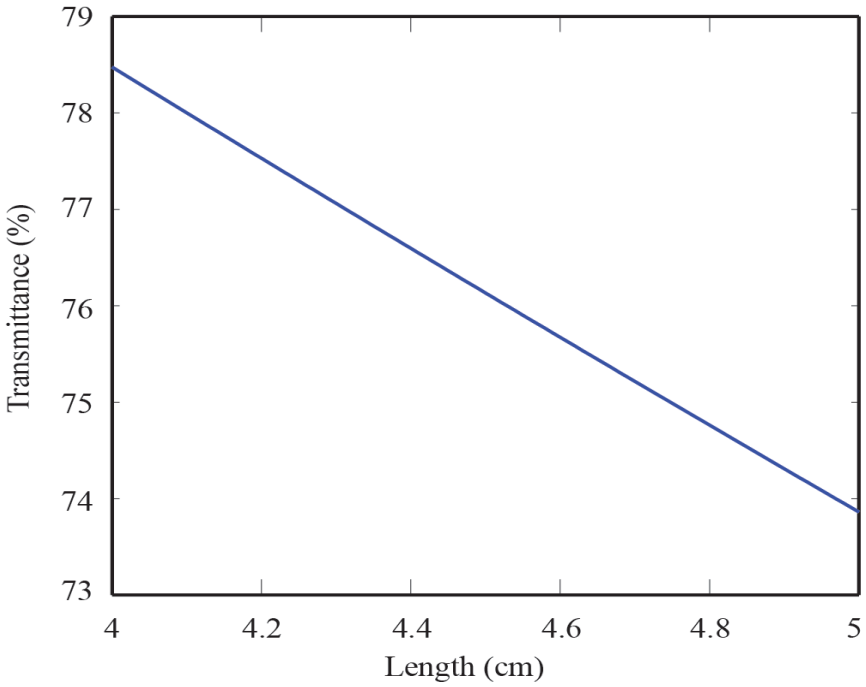

Figure 3-10: Transmittance vs. Path Length for Cargille Fluid 50350
over 4 cm to 5 cm

We are interested in knowing the attenuation of the beam as it travels through the absorbing medium (Cargille Fluid 50350). This phenomenon can be understood by plotting the transmittance (%) against length of the beam path in this absorbing medium. Graph in figure 3-9 shows that, transmittance of the UV light passing through Cargille Fluid 50350, decreases exponentially with the thickness of liquid layer. As shown in figure 3-10, for the path length of 4-5cm, the transmittance decreases almost linearly, dropping from 78% at 4 cm to 73% at 5 cm.

3.5 Contrast Analysis:

From the discussion in the last section, we know that the intensity of the two beams interfering on the substrate varies as the distance travelled by each arm of light is different. This difference is further accentuated for the Cargille Fluid 50350, as the intensity decreases exponential with the distance travelled, due to absorption of light. This causes the two interfering beams to have slightly different intensity.

The absolute intensity of the interference pattern is less critical and lower intensity can be accounted for by increasing the exposure time. However, it is critical to differentiate between the exposed and unexposed area. This differentiation is partly the function of the design of photoresist and it also depends on the high and low intensity regions in the aerial image.

Figure 3-11 shows the intensity as a function of position on the substrate. For high contrast, the minimum is zero and the maximum value is 1. So there will be clear distinction between the exposed and unexposed regions. But for the low contrast case, the minimum and the maximum values are shifted and the average remains same. Here, it will be difficult to differentiate between exposed and unexposed regions. This phenomenon can be quantified with a parameter known as contrast or visibility (V).

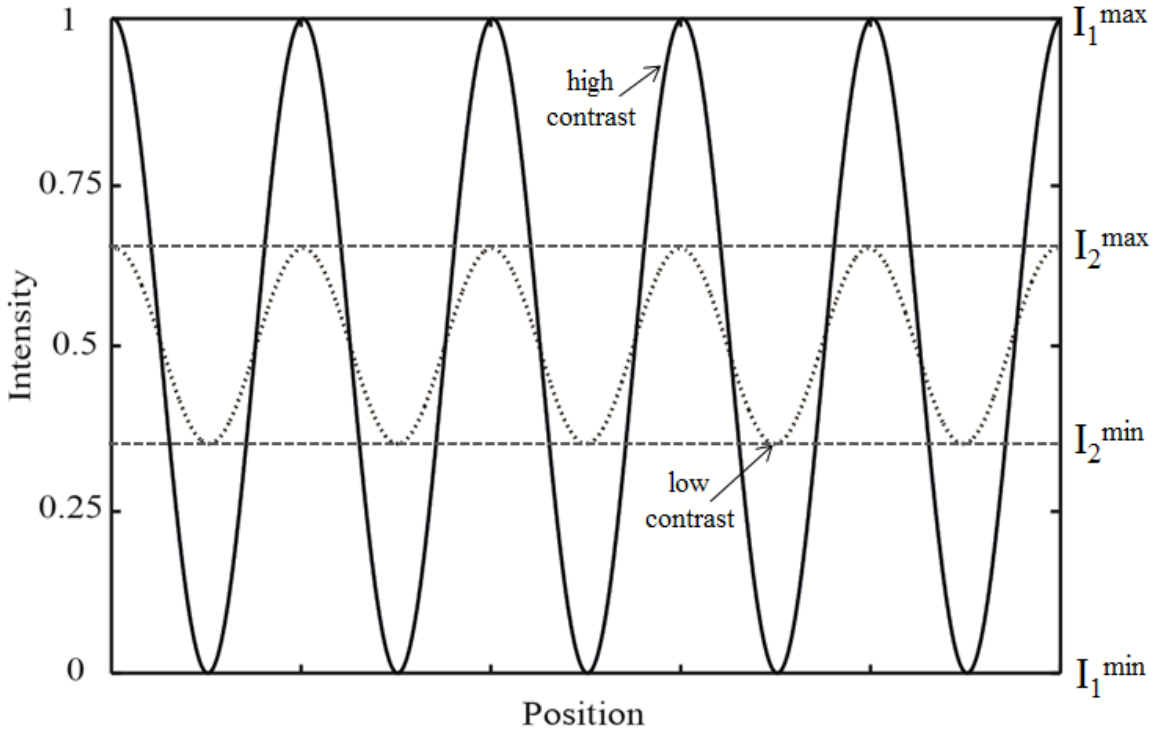

Figure 3-11: Intensity as a function of position

$$V = \frac{I_{max} - I_{min}}{I_{max} + I_{min}} \tag{3.3}$$

I_{max} and I_{min} values can be calculated using equation (2.15) by putting 1 and -1 respectively for cosδ.

$$I_{max} = I_1 + I_2 + 2\sqrt{(I_1 I_2)} \tag{3.4}$$

$$\mathrm{I}_{\min} = I_1 + I_2 - 2\sqrt{(I_1 I_2)} \tag{3.5}$$

Substituting these two equations in equation (3.3), we get

$$V = \frac{2\sqrt{(I_1 I_2)}}{I_1 + I_2} \tag{3.6}$$

From equation (3.6), it is clear that, the contrast is maximized (i.e. equal to 1) when both the beams have same intensity. Contrast goes on decreasing with the increased difference between the intensities of two interfering beams. With higher contrast, exposed and unexposed regions can be easily distinguished.

Understanding the contrast behavior for the samples made in Cargille fluid 50350 is important, as, unlike air and DI water, this immersion fluid absorbs the UV light and the transmittance decreases exponentially with the thickness of the liquid layer. Figure 3-12 shows the contrast plotted against the width of the sample. Appendix 1 includes mathematical derivation of contrast calculation.

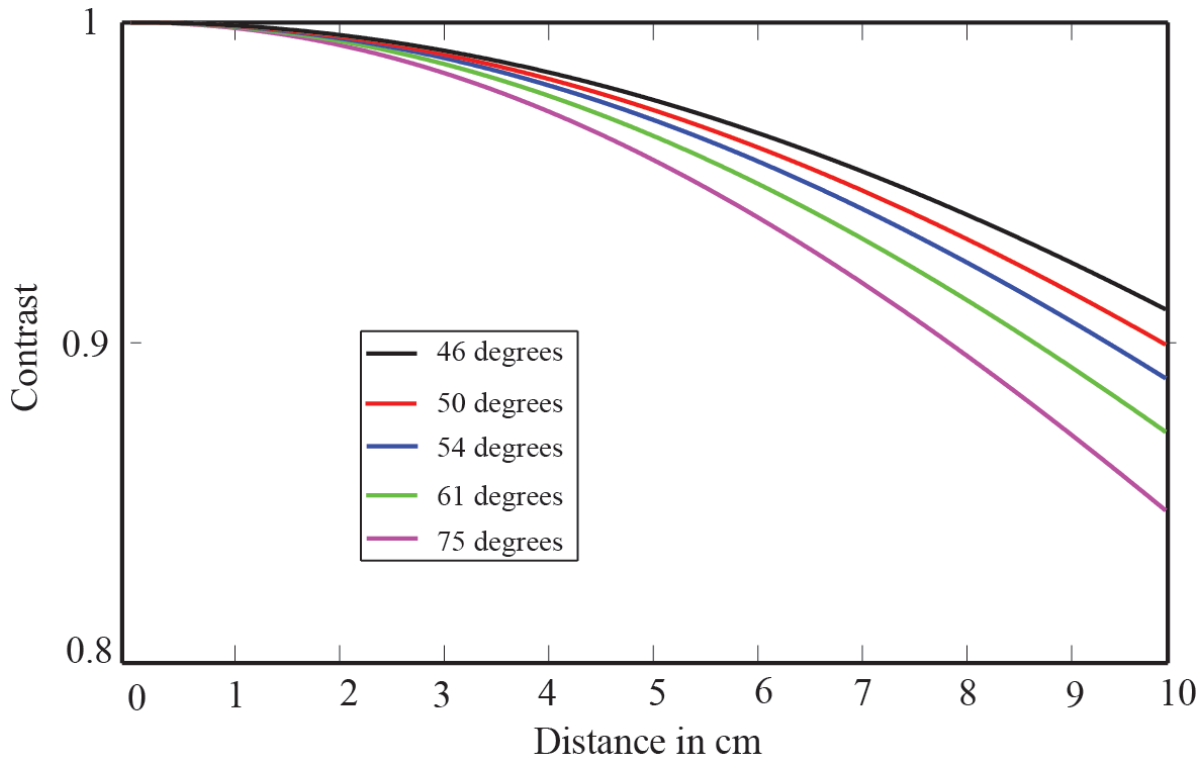

Figure 3-12: Contrast plotted against the substrate width for Cargille Fluid 50350

From the graph, we notice that, as the angle of incidence goes on increasing, contrast decreases. This is due the increase in relative distance travelled by two interfering beams. It is clear that, for the smaller size of the sample, the contrast remains almost same for a wide range of angle of incidence. For the experiments carried out the sample size ranges from 2 cm to 3 cm, over which the contrast is good and it is possible to get consistent periodic structure over a larger part of the sample. As the contrast is high, it is possible to use the immersion fluids with higher absorption coefficients; having higher refractive indices than the one used in these experiments. This will help to make structures with even smaller

period. This graph also signifies that, it is difficult to get consistent periodic structures over a larger sample, as the contrast decrease. To address this issue, we will have to use less absorbing immersion fluid. To get smaller period over a very large area, it is necessary to develop immersion fluids with low absorption and high refractive index.

Chapter 4 Fabrication of the Sub Wavelength Periodic Structure

This section will cover the fabrication steps involved in making sub wavelength periodic structures. Initial part of the chapter will cover the stack design for interference lithography. It is then followed by stack design for DI water for different periods. The experimental results obtained at different angles of incidence will then be compared with the theoretical model to know the system variability. Similar sequence will then be followed for Cargille Fluid 50350, and the results will be discussed. The chapter will be concluded with the comparison of results for air, DI water and Cargille Fluid 50350.

4.1 Interference Lithography Stack Design:

In chapter 2, we discussed about the interference of two beams to form an intensity pattern, which will then be received by the photoresist. However, in practice, it is four beams interference within the photoresist layer as depicted in figure 4-1. Some portion of the light incident on photoresist will be reflected and remaining will be transmitted through the photoresist. The transmitted light will be reflected at the second interface as shown in the figure 4-1. This reflected light will degrade the quality of structure that we will be getting after developing the photoresist.

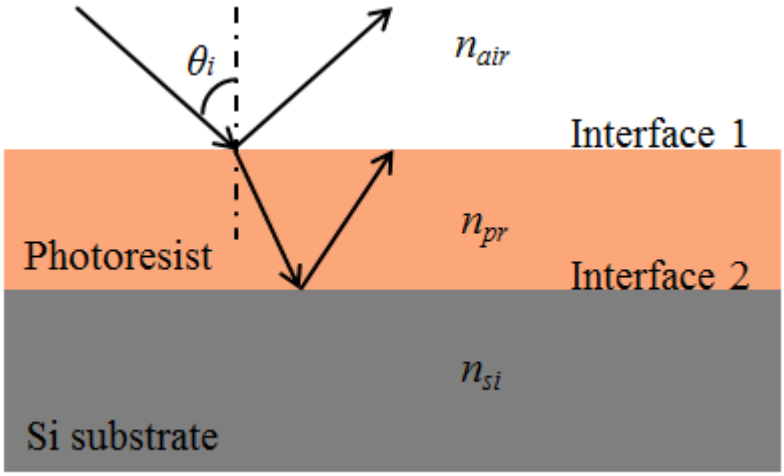

Figure 4-1: Schematic of beam reflection in a stack without ARC

We are interested in creating straight wall structures and this can be achieved by eliminating the reflection from the interface 2. The reflection at the interface 2 can be eliminated by adding an anti-reflection coating (ARC) layer after the photoresist. It is necessary to optimize the thickness of ARC layer, which is the function of the desired period of the structure and thickness of the photoresist layer. A computer program is used to find the optimum thickness of the ARC layer [18].

Figure 4-2 shows the stack design for making periodic structures using ARC. Here, refractive index of the air at the first interface is 1. In case of immersion interference lithography, the light has to travel through the high refractive index medium before it is incident on the photoresist layer. So, it becomes important take into account the refractive index of the medium, while finding the optimum thickness of the ARC layer. Failure to account for the refractive index of the medium results in wrong value of ARC thickness.

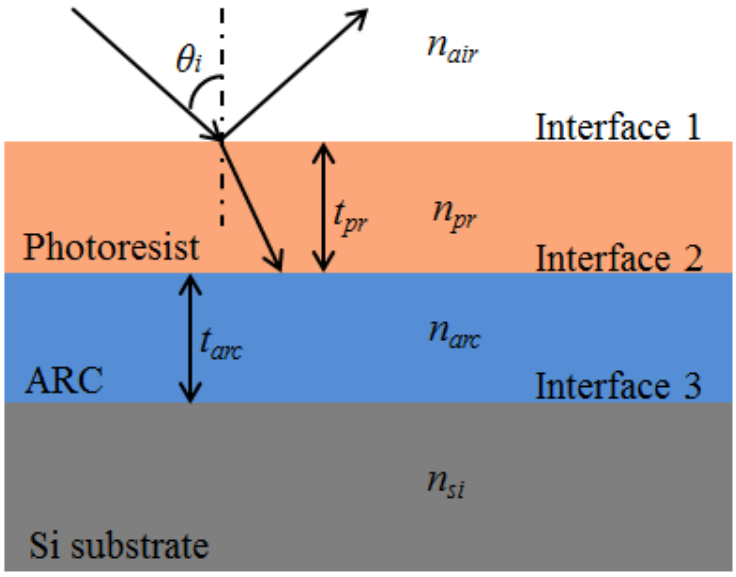

Figure 4-2: Schematic of beam reflection in a stack with ARC

4.2 Stack Design and Experimental Results for DI water:

Initial experiments are carried out using DI water to check the feasibility of the set-up. DI water is the most commonly used immersion fluid due to easy availability and also due to its 100% transmittance in UV range. It has a refractive index of 1.33 at 325 nm wavelength, which will effectively reduce the wavelength to ~ 244 nm. DI water has low viscosity, is stable under 325 nm wavelength exposure and it does not react with the optical equipment's used for experiment [22, 23].

The stack design for immersion interference lithography is different from that used for exposure in air using Lloyd's mirror interferometer. The thickness of the ARC layer changes due to the high refractive index medium used. Table 4-1 lists the materials, their respective thicknesses and the refractive indices;

Table 4-1: Material characteristics for ARC thickness optimization, while using DI water as immersion fluid.

Layer #	Medium	Thickness	Refractive Index
1	DI water	semi-infinite	1.33
2	Photoresist (Sumitomo PFI-88)	50 nm	1.79-0.02i
3	ARC (ARC-i-CON-7)	$\mathbf{t_{arc}}$	1.445-0.3402i
4	Silicon substrate	semi-infinite	4.68-2.03i

A computer program is used with some modifications, to accommodate for the refractive index of immersion media, to calculate the thickness of ARC layer for different periods of the structures. The period of the structure is varied by changing the angle at which light is incident on the system. Table 4-2 summarizes the optimum ARC layer thicknesses for different periods.

Table 4-2: ARC layer thickness for different periodicity, for DI water as immersion fluid

Period (nm)	Angle of incidence (θ_i degrees)	ARC thickness $\mathbf{t_{arc}}$ (nm)
140	60.77	98.0
150	54.54	93.2
160	49.78	89.6
170	45.95	87.2

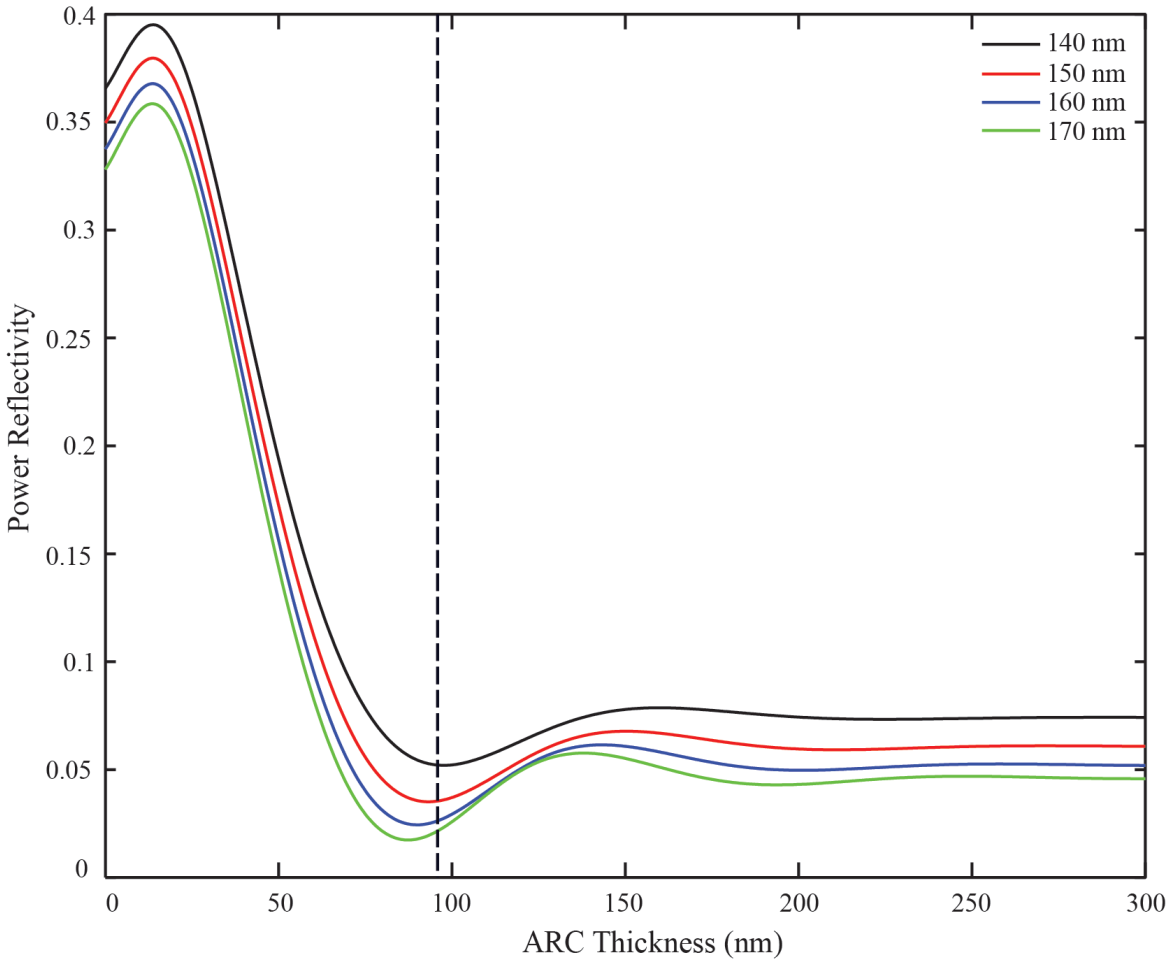

Figure 4-3: Reflectivity vs. ARC thickness for DI water

Figure 4-3 shows the ARC thickness for different periods plotted against the power reflectivity. It is important to choose the ARC thickness which gives the minimum power reflectivity for given period. From figure 4-3 it is also clear that, as the period of the structure increases, the power reflectivity and the corresponding ARC thickness decreases. Generally, it is advisable to the power reflectivity below 1%, but as is clear in the figure, the lowest power reflectivity is for 170 nm period and it is around 1.7%. With higher reflectivity, it

becomes difficult to get a good structure having straight wall on the gratings, as the increased reflection from the interface between photoresist and ARC reduces the contrast. This problem can be reduced by using the ARC having higher refractive index. Here, we are reducing the thickness of photoresist layer to account for higher reflectivity.

The experiments using Di water as immersion fluid are carried out. Following figure shows the results obtained for 140 nm period at an angle of incidence of ~61°. Figures (a) and (b) are the top view of the sample and, (c) and (d) indicate the cross-section of the sample.

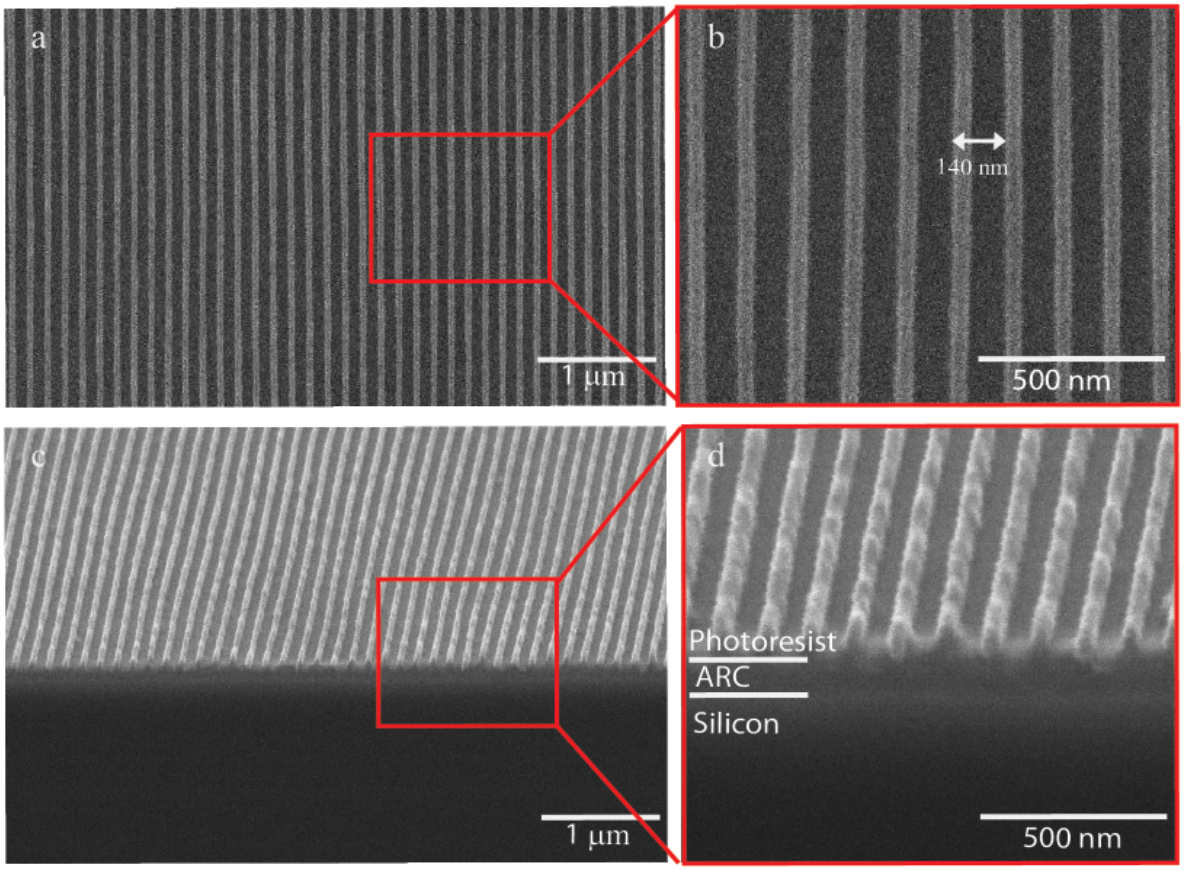

Figure 4-4: 140 nm period using DI water as immersion fluid

Following images show the results obtained for 150 nm, 160 nm and 170 nm respectively;

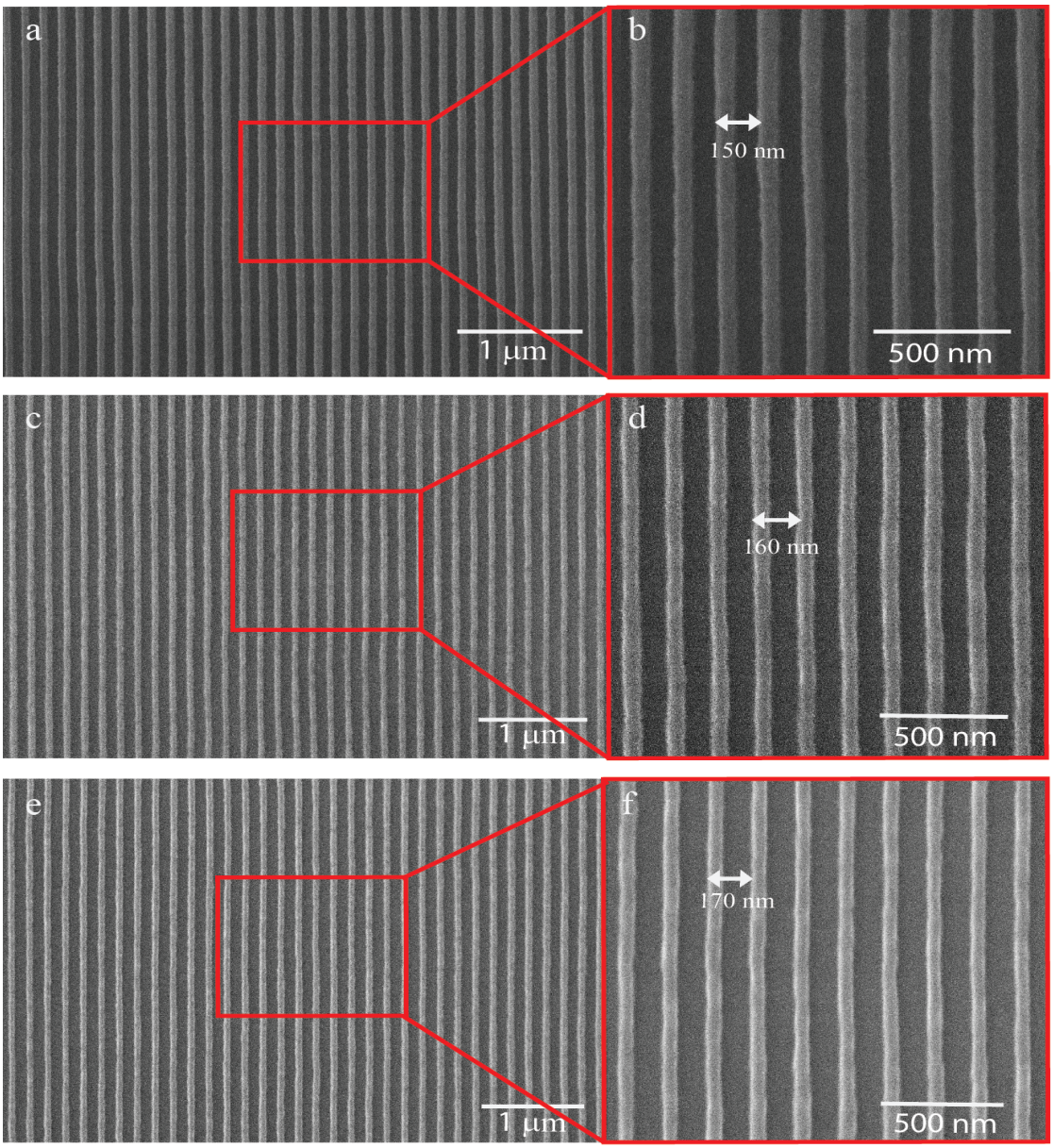

Figure 4-5: Results for DI water as immersion fluid

Using the proposed setup, it is possible to get the desired period of the structure over microscopic area.

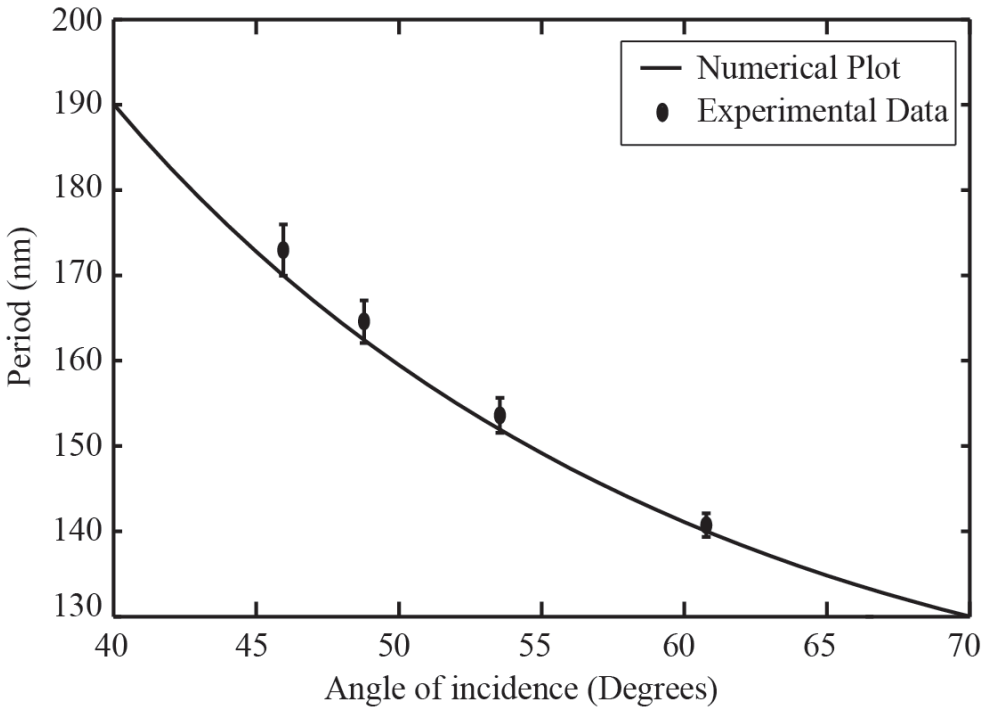

Figure 4-6: Period vs. Angle of incidence with DI water as immersion fluid

With the proposed setup, it is possible to get the periodicity of the structure over a wide range, by changing the angle of incidence. The smallest period produced will be reduced by 1.33, compared to the results obtained in air. Figure 4-6 shows the plots for numerical and experimental data. As we can notice from the plot, there is slight variation in periodicity. This variation may be because of manual error while adjusting the angle of the container.

4.3 Stack Design and Experimental Results for Cargille Fluid 50350:

From equation (2-.17) it is clear that, the periodicity of the structure is a function of the refractive index of the medium through which light travels. To exploit this, we decided to use an immersion fluid with higher refractive index than DI water. But unlike DI water, high refractive index fluids absorb light and that put the limitation over the use of immersion fluid. Cargille Fluid 50350 has a refractive index ~ 1.5057 and its attenuation coefficient is 0.0606, which is found experimentally in section 3.3. For the proposed set, the path length of the beam varies in the range of 4 cm to 5 cm, depending on the angle of incidence. For this path length, the intensity of the light transmitted, varies from 73% to 78% of the incoming beam intensity. This drop in intensity is compensated by increasing the exposure time. Though we notice a drop in the intensity, the contrast remains high for smaller samples, as the relative path difference between two interfering beams is small.

These experiments are carried out using the parameters as used for DI water, except refractive index of the medium. ARC thickness for different angles of incidence is calculated using the same computer program. Table 4-3 summarizes this data;

Table 4-3: ARC layer thickness for different periodicity, for Cargille fluid 50350.

Period (nm)	Angle of incidence (θ_i degrees)	ARC thickness $\mathbf{t_{arc}}$ (nm)
120	64.52	97.4
130	56.12	91.4
140	50.43	86.0
150	45.95	82.4

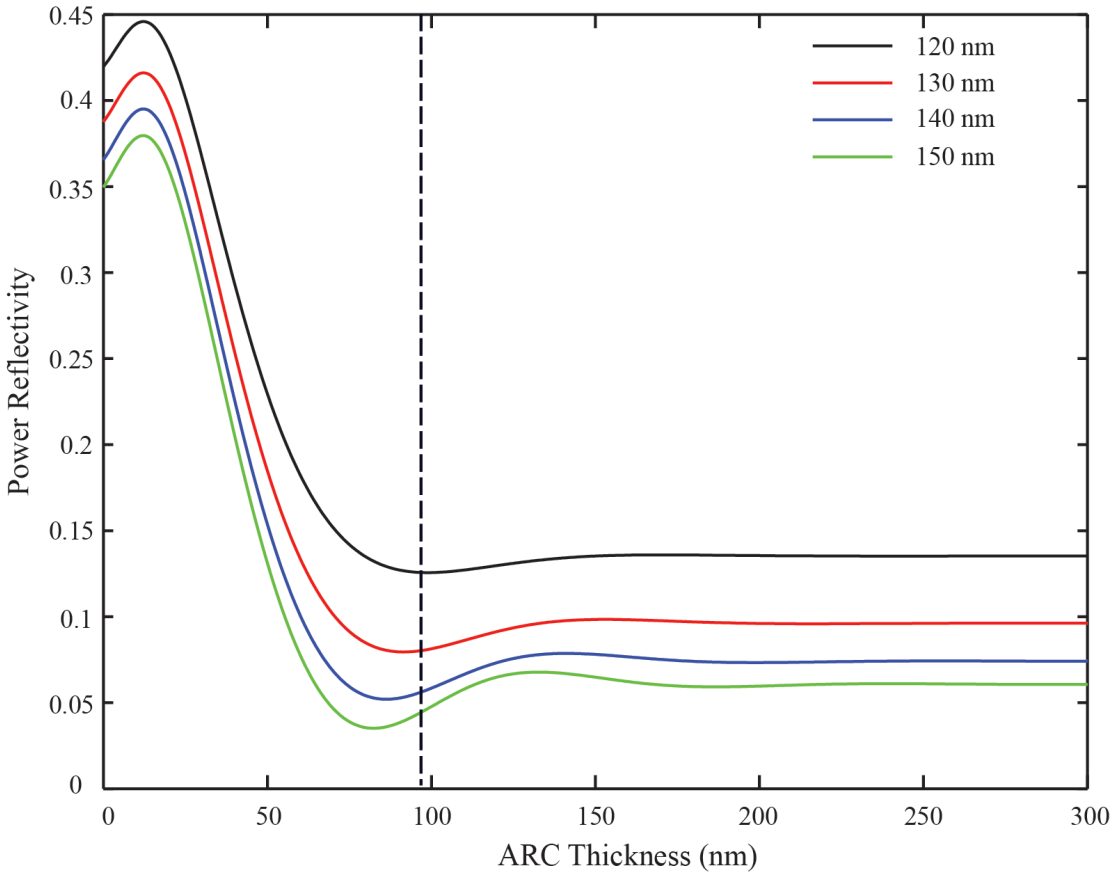

Figure 4-7: Reflectivity vs. ARC thickness for Cargille Fluid 50350

Figure 4-7 shows the ARC thickness for different periods plotted against the power reflectivity, while using Cargille Fluid 50350 as immersion fluid. We choose the ARC thickness which gives minimum reflectivity. Figure 4-7 follows similar trend for period, reflectivity and ARC thickness, as discussed in previous section. It is also clear that, while using Cargille Fluid, the power reflected from the ARC layer has increased. So, it becomes necessary again to use thinner layer of photoresist. We have used photoresist thickness of 50 nm to perform these experiments.

Following figure shows the results obtained for 120 nm period at an angle of incidence of ~64.5. Figures (a) and (b) are the top view of the sample and, (c) and (d) indicate the cross-section of the sample. Figure (d) also shows the different layers on the sample.

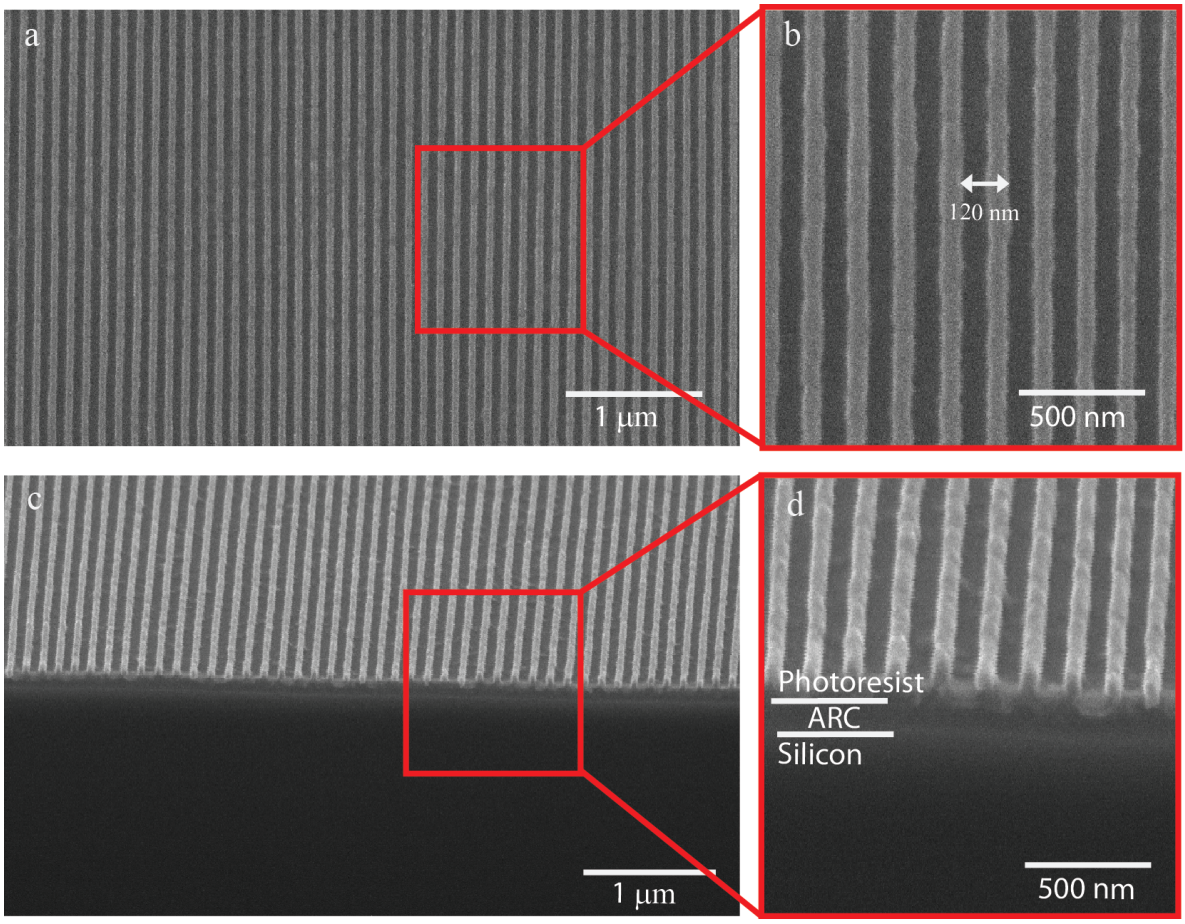

Figure 4-8: 120 nm period using Cargille Fluid 50350 as immersion fluid

Following images show the results obtained for 130 nm, 140 nm and 150 nm respectively;

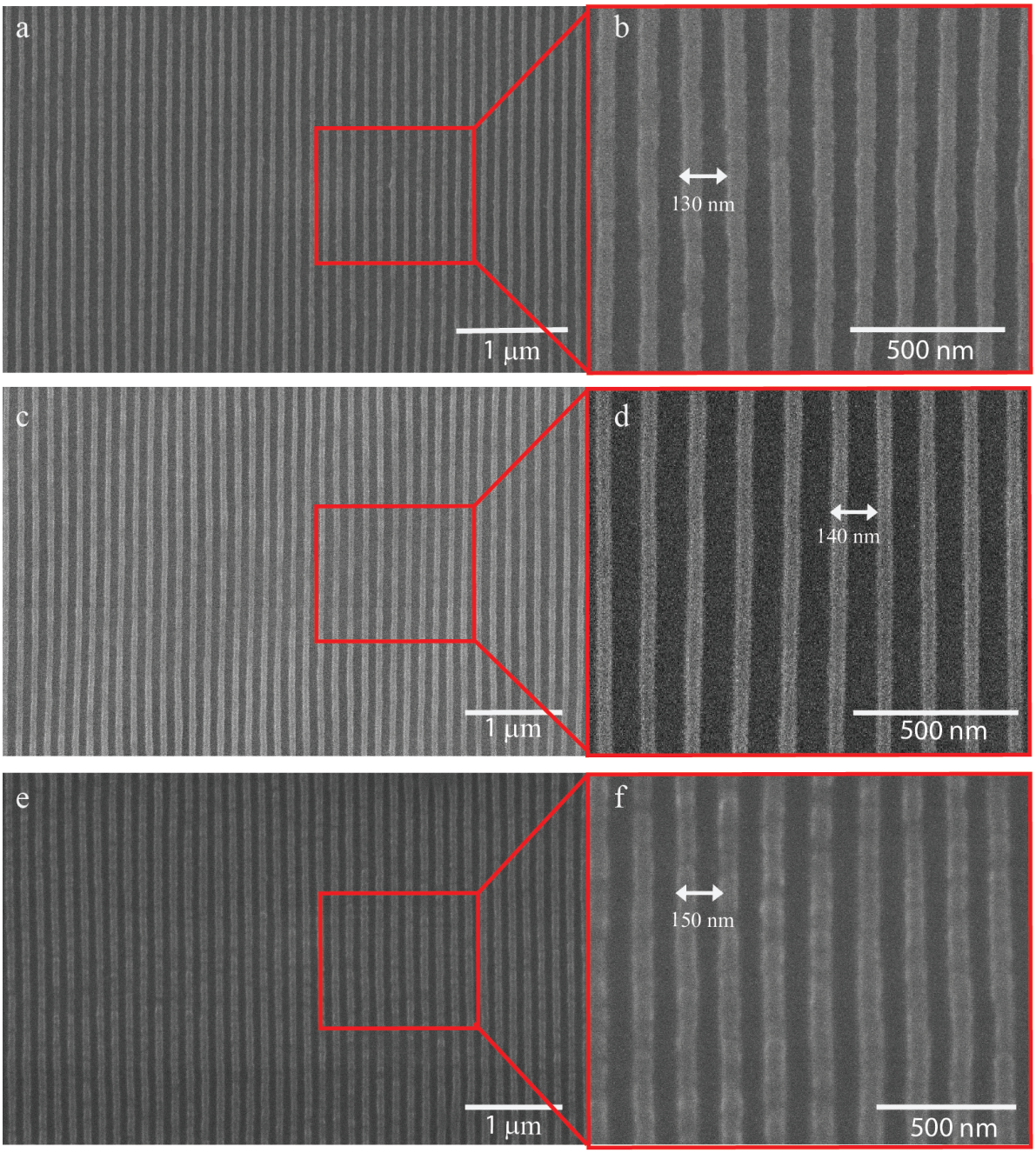

Figure 4-9: Results for Cargille Fluid 50350 as immersion fluid

The system designed is very flexible and can be adjusted to very steep angle of incidence. To check this, we have carried out the experiment with angle of incidence of 75°. The results of this experiment are shown in figure 4-11. The line width of this structure is about 50 nm. At such a large angle of incidence, it is difficult to get a good exposure over a large area, as the sample is not at the center of the light source. This problem can be solved by building a larger container.

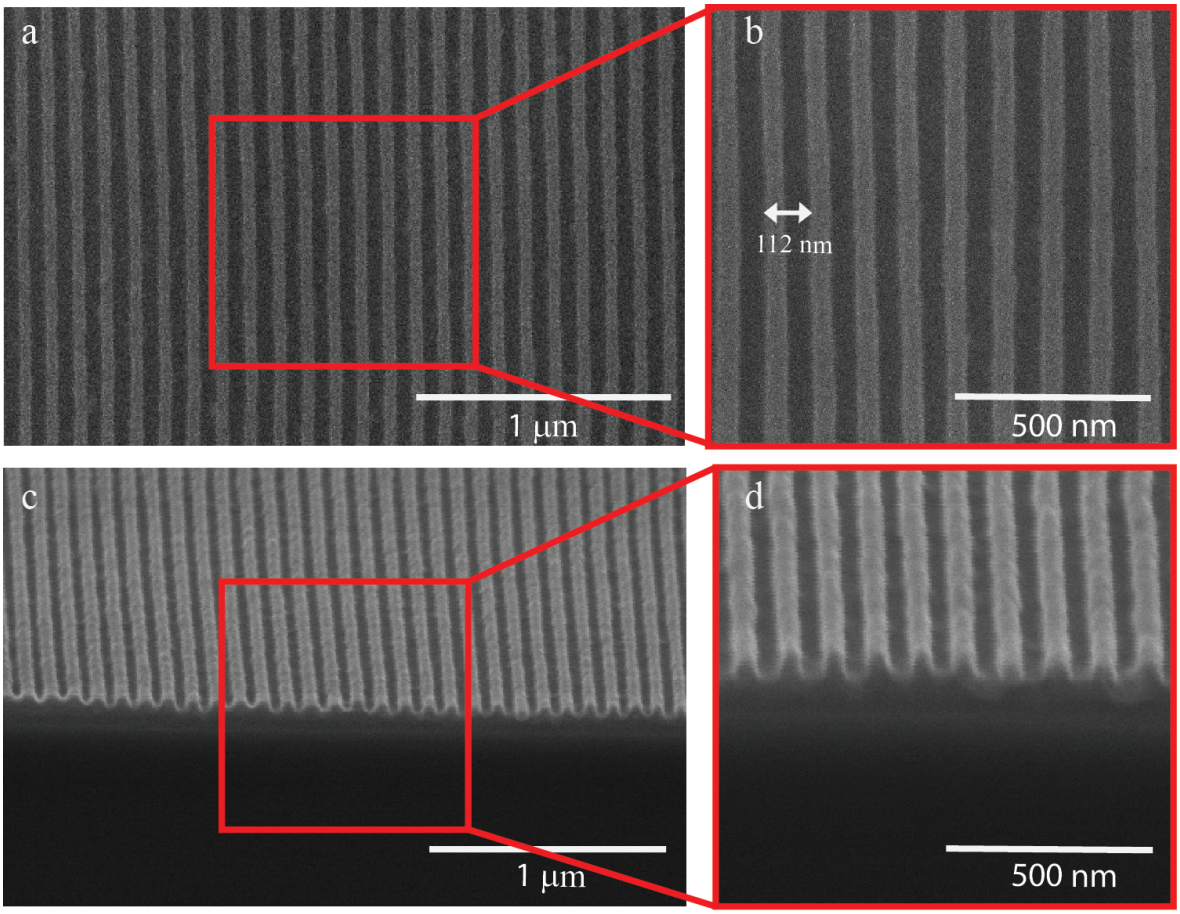

Figure 4-10: 112 nm period using Cargille Fluid 50350 as immersion fluid

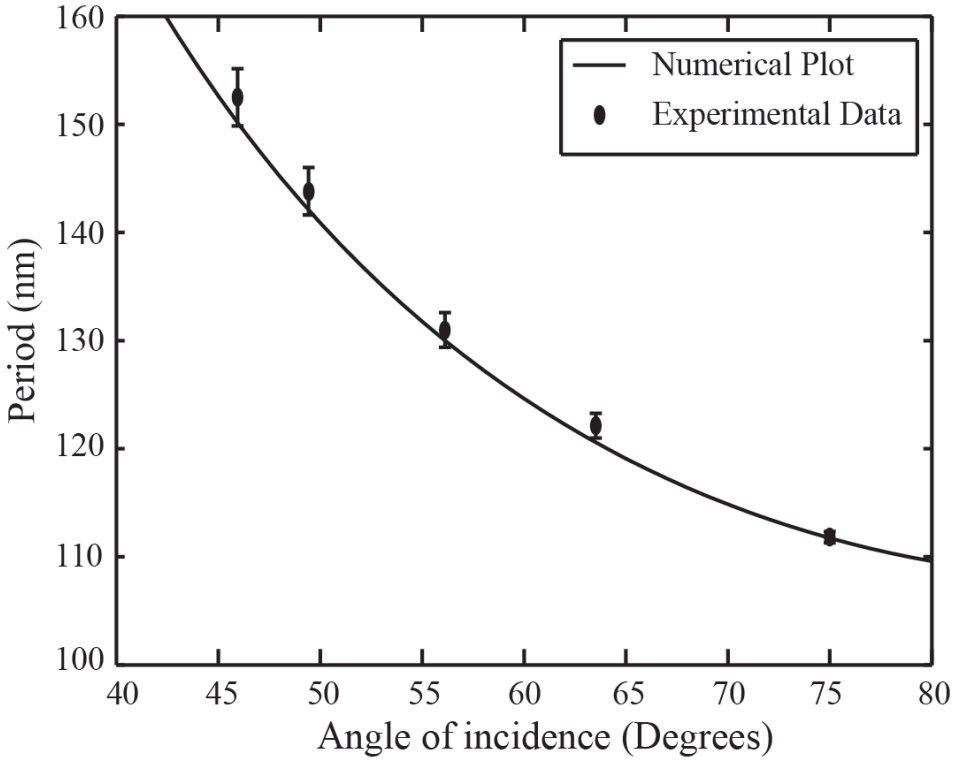

Figure 4-11: Period vs. Angle of incidence with Cargille Fluid 50350 as immersion fluid

Figure 4-11 plots the experimental data and the numerical trend for period vs. angle of incidence comparison. The experimental data closely follows the numerical results and slight variations are the result of manual error during angle adjustment.

4.4 Period Comparison between Air, DI Water and Immersion Oil:

In last two sections we have demonstrated that the proposed setup can be successfully used to fabricate sub-wavelength periodic structures. By changing the medium through which the light travels, we have been able to make smaller structures. Using a laser having 325 nm

wavelength, we have been able to produce the periodic structure of 112 nm. Figure 4-12 summarizes the results for air, DI water and Immersion Oil. The experimental results are in good agreement with the numerical plat and the small variations in the period are the result of error in angle adjustment.

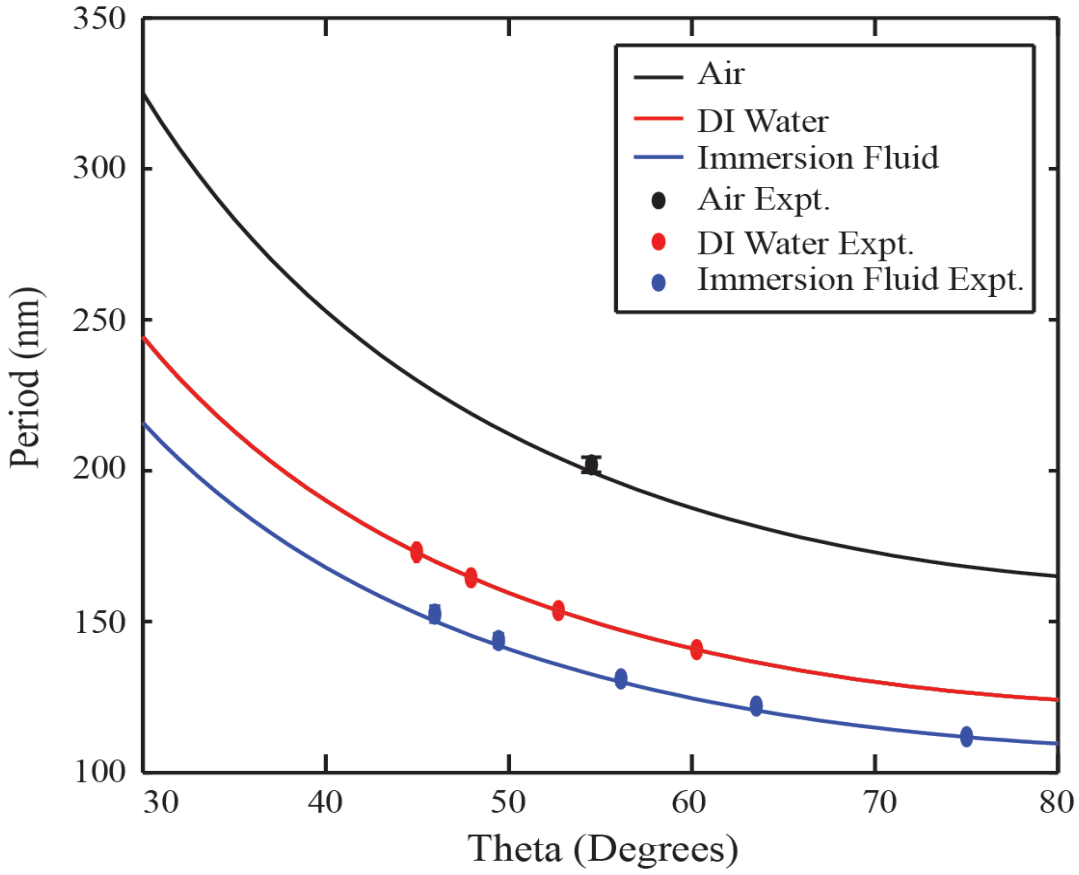

Figure 4-12: Period reduction with immersion

We notice that, the periodicity decreases as the refractive index of the medium increase. It is possible with this proposed setup to produce structures having even smaller period by using the immersion fluids with higher refractive index. In section 3.5, we noticed

that the contrast will be better for smaller samples with higher refractive index fluid, as the difference in the path length of two interfering beams remains low. But contrast will be poor for larger samples as the difference in the relative distance travelled by both interfering beams increases. This issue can be addressed by using immersion fluid with lower absorption. Currently, there is a trade-off while selecting the immersion fluid, as we can either get higher refractive index and higher absorption or vice versa.

Figure 4-13 shows the microscopic image comparison for the samples made using different media. Images (a), (c) and (d) are the microscopic images for samples made using air, DI water and immersion oil respectively, as the media through which light travels before it is incident on the sample. SEM images are also shown for all three samples to enable comparison of structures obtained using different media. The difference in color of microscopic images is the result of different thickness of photoresist and ARC layer.

Image (b) shows the SEM image for 200 nm period structure, made in air. The grating lines obtained have very good spatial coherence and it has been observed that the gratings can be produced over a very large area (cm^2). But the smallest periodicity that can be produced in air using a 325 nm laser is around 190 nm. So, to get a smaller period, we either have to use smaller wavelength of light or a medium with higher refractive index.

To get smaller period, we have used high refractive index fluids, DI water and Cargille Fluid 50350. The microscopic images for the samples made in DI water and Immersion oil are shown in (c) and (e). It is observed that the sample made in DI water has a formation of densely packed ring like structures. The immersion oil sample too has similar

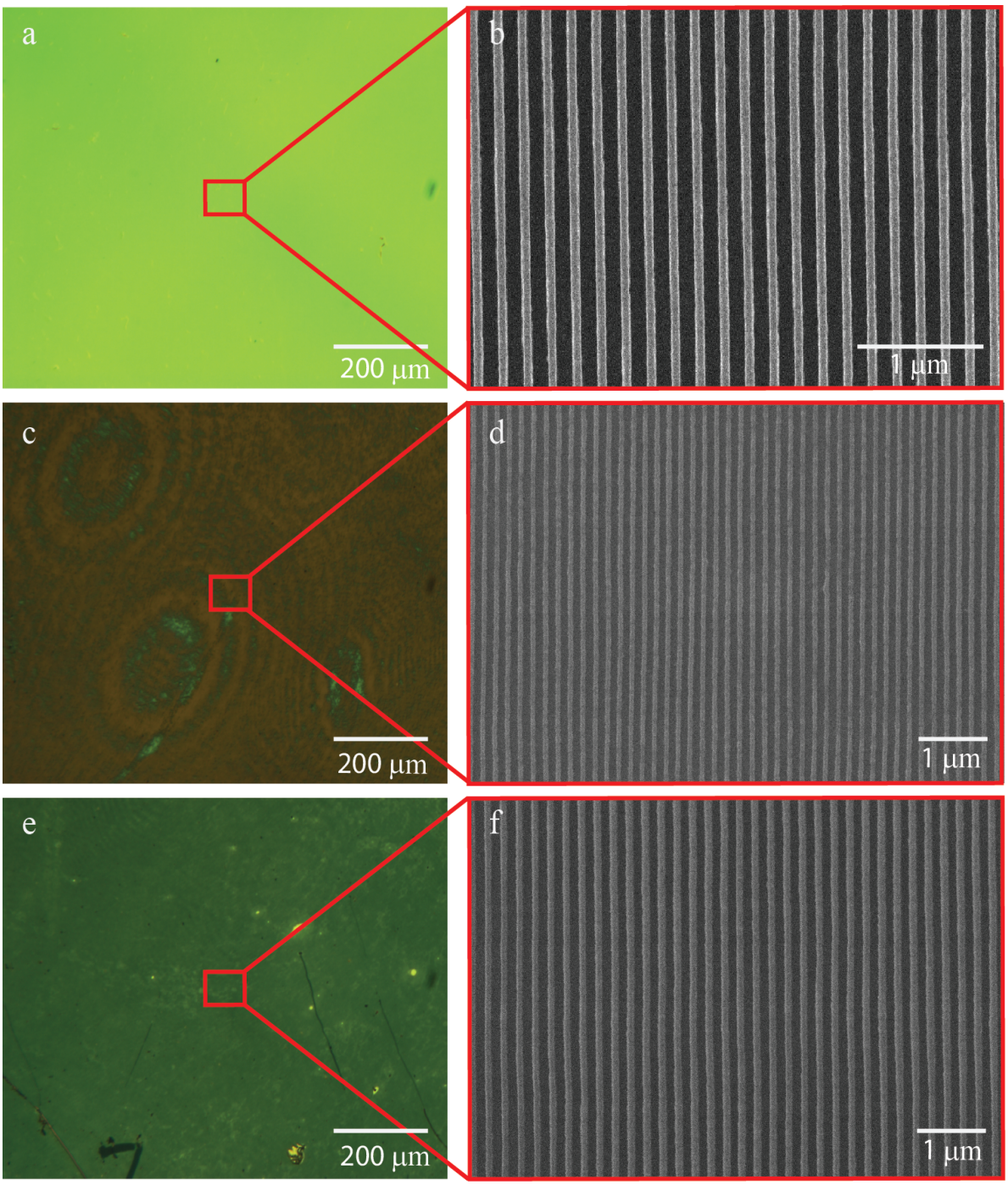

Figure 4-13: Microscopic image comparison (a) Air sample with 200 nm period, (b) SEM image for Air sample, (c) DI water sample for 150 nm period, (d) SEM image for DI water sample, (e) Immersion Oil sample with 150 nm period, (f) SEM image for Immersion Oil sample

rings but the density is much less than the sample made in DI water. This formation of rings is the result of scattering caused by the particles present in immersion fluid, as these experiments are carried out in a lab. This problem can be addressed by using a highly purified immersion fluid and conducting the experiments in clean room.

Images (d) and (f) are the SEM images of a 150 nm sample made in DI water and Cargille Fluid respectively. Samples having same periodicity are used for better comparison of effect of immersion fluids on the resulting structure. From the SEM image of the DI water sample we can notice that, the line width of the structure varies a lot, and could be attributed to the scattering caused by the large number of particles present in DI water. For the sample made using the Cargille Fluid 50350, the line width is constant everywhere. The sample made in immersion oil gives a very good spatial coherence. Also, it gives higher spatial resolution than air as a result of high refractive index (n = 1.51). Using the immersion oil in the system designed here, we have been able to fabricate gratings over a microscopic region. By using a higher container and the immersion fluid with smaller absorption coefficient, it is possible to fabricate the gratings over a very large area.

Chapter 5 Conclusion

We have successfully combined the immersion lithography with the Lloyd's mirror interferometer to fabricate sub-wavelength periodic gratings, with high spatial coherence, over several microns of area, with very low defects. Unlike the currently available solid-liquid immersion lithography methods, the proposed method is all liquid and is suitable for making the sub-wavelength periodic gratings over a larger area. The setup designed is very compact and requires minimum adjustments to get a large periodicity range. Also, it does not require any special mechanism to maintain a continuous layer of fluid between the wafer and optical lens. We make use of gravity to maintain immersion fluid against the wafer, this arrangement rules out the possibility of formation of air pockets, thereby eliminating the possible source of defects. The microscopic image comparison of samples indicates that, the immersion interference lithography using a clean immersion fluid is comparable with the results obtained using Lloyd's mirror interferometer in air. This fact underlines the commercial potential of this system to make sub-wavelength periodic structures.

This setup is very economical considered to the 193 nm scanner used in semiconductor industry to make sub-wavelength periodic structures. We have been able to fabricate gratings with a smallest period of 112 nm using 325 nm light. Using this setup, it is possible to get desired period of gratings with very high precision. Some variation observed in periodicity of gratings is the result of manual error in adjusting the angle of incidence. This problem can easily be solved by making use of automatic controls to adjust the angle.

It is possible to fabricate structures with even smaller periodicity. It can be achieved by using a laser having smaller wavelength and by using immersion fluid with higher refractive index. Existing immersion fluids with higher refractive index suffer from increased absorption at smaller wavelength of light. The contrast calculations show that for small samples, it is possible to use high refractive index fluid, even if it means increased absorption. But for larger samples, we will have lower spatial coherence. So, it is necessary to develop the immersion fluids with lower absorption coefficient and higher refractive index.

For the experiments carried out, the photoresist thickness used is only 50 nm, to account for the higher values of reflected power from the photoresist-ARC interface. To use higher photoresist thickness, it is necessary to use an ARC with higher refractive index, which will reduce the reflected power at the interface. With increased photoresist thickness, we can use this as a mask during reactive ion etching process. The periodic nanostructured gratings produced using IIL can be useful in x-ray and extreme UV spectroscopy, and to make templates for sub assembly. The future work involves making 2D patterns in the photoresist using the IIL. Due to the smaller periodicity, the structure produced after RIE will have densely packed Nano cones, for a 2D pattern. These closely packed Nano cones will have improved hydrophobicity/hydrophilicity and better anti-reflection property. It will be also possible to pack more number of electrodes for information collection in biomedical applications. The increased number of Nano cones or the reduced periodicity of the gratings will provide a better surface to volume ratio, which could be very useful in gas sensing

applications. Having the smaller grating period structure on the piezoelectric device might induce more stress in the device, thereby improving the results obtained from such devices.

REFERENCES

[1] Whitesides, George M., John P. Mathias, and Christopher T. Seto. 1991. *Molecular Self-Assembly and Nanochemistry: A Chemical Strategy for the Synthesis of Nanostructures*.

[2] Winfree, E, F Liu, L A Wenzler, and N C Seeman. 1998. "Design and Self-assembly of Two-dimensional DNA Crystals." *Nature* 394 (6693) (August 6): 539–544. doi:10.1038/28998.

[3] Chang, C.-H., L. Tian, W. R. Hesse, H. Gao, H. J. Choi, J.-G. Kim, M. Siddiqui, and G. Barbastathis. "From Two-Dimensional Colloidal Self-Assembly to Three-Dimensional Nanolithography." *Nano Letters* 11, no. 6 (June 8, 2011): 2533–2537.

[4] Chang, Chih-Hao, Hyun Jin In, Satoshi Takahashi, Martin Deterre, Hyungryul Johnny Choi, Kevin W Gotrik, and George Barbastathis. "Assembling Nanoparticle Catalysts with Nanospheres for Periodic Carbon Nanotube Structure Growth." *Nanotechnology* 22, no. 3 (January 21, 2011): 035301.

[5] Chang, Chih-Hao, Jose A. Dominguez-Caballero, Hyungryul J. Choi, and George Barbastathis. "Nanostructured Gradient-index Antireflection Diffractive Optics." *Optics Letters* 36, no. 12 (June 15, 2011): 2354–2356.

[6] Lee, Jae-Hwang, Jonathan P. Singer, and Edwin L. Thomas. "Micro-/Nanostructured Mechanical Metamaterials." *Advanced Materials* 24, no. 36 (2012): 4782–4810.

[7] Crommie, M F, C P Lutz, and D M Eigler. 1993. "Confinement of Electrons to Quantum Corrals on a Metal Surface." *Science (New York, N.Y.)* 262 (5131) (October

8): 218–220. doi:10.1126/science.262.5131.218.

[8] Piner, Richard D., Jin Zhu, Feng Xu, Seunghun Hong, and Chad A. Mirkin. 1999. "'Dip-Pen' Nanolithography." *Science* 283 (5402) (January 29): 661–663. doi:10.1126/science.283.5402.661.

[9] Bard, Allen J., Guy Denuault, Chongmok Lee, Daniel Mandler, and David O. Wipf. 1990. "Scanning Electrochemical Microscopy - a New Technique for the Characterization and Modification of Surfaces." *Accounts of Chemical Research* 23 (11) (November 1): 357–363. Doi: 10.1021/ar00179a002.

[10] Betzig, Eric, and Jay K. Trautman. 1992. "Near-Field Optics: Microscopy, Spectroscopy, and Surface Modification beyond the Diffraction Limit." *Science* 257 (5067) (July 10): 189–195. doi:10.1126/science.257.5067.189.

[11] Xia, Y, JA Rogers, KE Paul, and GM Whitesides. 1999. "Unconventional Methods for Fabricating and Patterning Nanostructures." *Chemical Reviews* 99 (7): 1823–1848.

[12] Eugene Hecht, Optics, Addison-Wesley, 2002.

[13] Max Born, and Emil Wolf, Principals of Optics, Cambridge university press, 1999.

[14] Grant R Fowles, Introduction to modern optics, Dover publications, 1975.

[15] Michael E Walsh, On the design of lithographic interferometers and their application, PhD thesis, Massachusetts Institute of Technology, Department of Mechanical Engineering, 2004.

[16] Smith H.I. 2001. "Low Cost Nanolithography with Nanoaccuracy." *Physica E* 11 (2): 104–109. doi:10.1016/S1386-9477(01)00184-9.

[17] Harry J Levinson, Principles of Lithography, SPIE press, 2005

[18] M. E. Walsh, nanostructuring magnetic thin films using interference lithography, M.S thesis, Massachusetts Institute of Technology, Department of Mechanical Engineering, 2000.

[19] de Boor, J., Kim, D. S. & Schmidt, V. Sub-50 nm patterning by immersion interference lithography using a Littrow prism as a Lloyd?s interferometer. *Opt. Lett.* **35**, 3450–3452 (2010).

[20] Bloomstein, T. M., Marchant, M. F., Deneault, S., Hardy, D. E. & Rothschild, M. 22-nm immersion interference lithography. *Opt. Express* **14**, 6434–6443 (2006).

[21] French, R. Immersion Lithography: Photomask and {Wafer-Level} Materials. *Annual Review of Materials Research* **39**, 93–126 (2009).

[22] Wei, Y. & Brainard, R. L. *Advanced Processes for 193-Nm Immersion Lithography*. (SPIE Press: 2009).

[23] Wei, Y. 193nm immersion lithography: Status and challenges. *SPIE Newsroom* (2007).doi:10.1117/2.1200703.0001

[24] Chang, C.-H., Zhao, Y., Heilmann, R. K. & Schattenburg, M. L. Spatial-frequency multiplication with multilevel interference lithography. *Journal of Vacuum Science & Technology B: Microelectronics and Nanometer Structures* **26**, 2135 (2008).

[25] Chang, C.-H., Zhao, Y., Heilmann, R. K. & Schattenburg, M. L. Fabrication of 50 nm period gratings with multilevel interference lithography. *Opt. Lett.* **33**, 1572–1574 (2008).

[26] Cheng, J. Y., Ross, C. A., Thomas, E. L., Smith, H. I. & Vancso, G. J. Fabrication of

nanostructures with long-range order using block copolymer lithography. *Applied Physics Letters* **81**, 3657–3659 (2002).

[27] Hambach, D., Schneider, G. & Gullikson, E. M. Efficient high-order diffraction of extreme-ultraviolet light and soft x-rays by nanostructured volume gratings. *Opt. Lett.* **26**, 1200–1202 (2001).

[28] Kanamori, Y., Sasaki, M. & Hane, K. Broadband antireflection gratings fabricated upon silicon substrates. *Opt. Lett.* **24**, 1422–1424 (1999).

[29] Keith, D. W., Schattenburg, M. L., Smith, H. I. & Pritchard, D. E. Diffraction of Atoms by a Transmission Grating. *Phys. Rev. Lett.* **61**, 1580–1583 (1988).

[30] Kim, D.-H. *et al.* Dissolvable films of silk fibroin for ultrathin conformal bio-integrated electronics. *Nature Materials* **9**, 511–517 (2010).

[31] Kowalski, M. P. *et al.* Near-normal-incidence extreme-ultraviolet efficiency of a flat crystalline anisotropically etched blazed grating. *Appl. Opt.* **45**, 1676–1679 (2006).

[32] Seely, J. F. *et al.* Efficiency of a grazing-incidence off-plane grating in the soft-x-ray region. *Appl. Opt.* **45**, 1680–1687 (2006).

APPENDICES

Appendix A

Contrast calculations for proposed setup

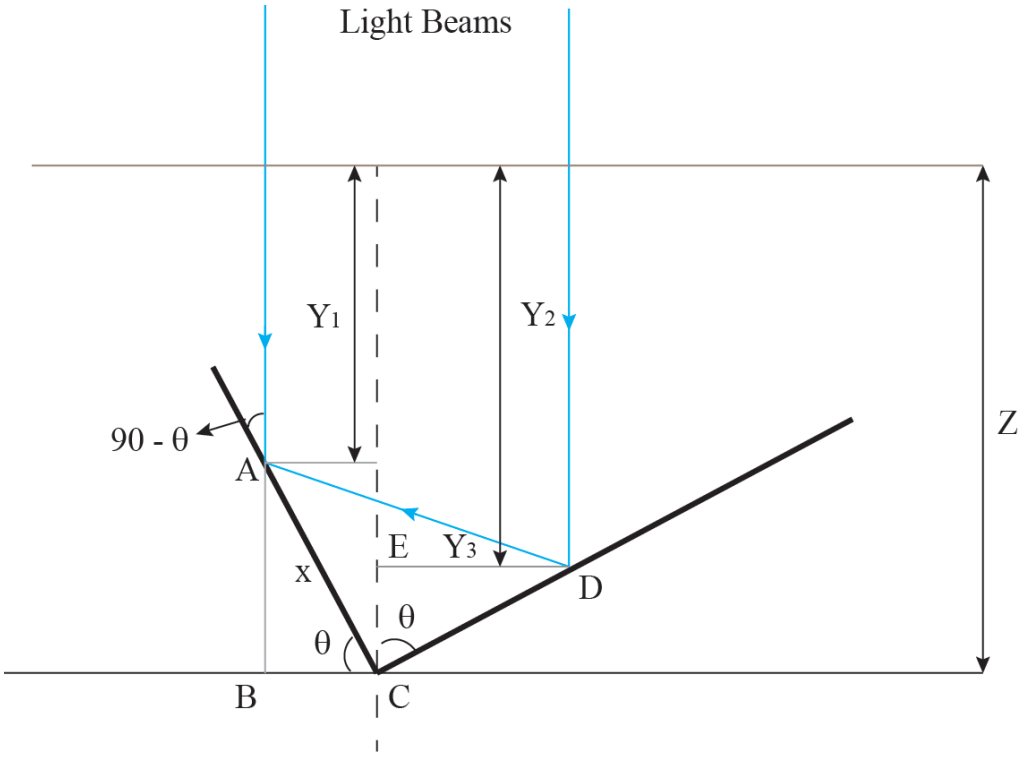

Figure A-1: Line diagram of container for contrast calculation

Z – Immersion fluid layer thickness (top of liquid layer is used as datum)

In ΔABC,

$$sin\theta = \frac{AB}{x}$$

$$AB = xsin\theta$$

$$BC = x\cos\theta$$

In ΔACD,

$$\tan(90-\theta) = \frac{CD}{x}$$

$$CD = xtan(90-\theta)$$

$$\cos(90-\theta) = \frac{x}{Y_3}$$

$$Y_3 = \frac{x}{\cos(90-\theta)}$$

In ΔCDE,

$$sin\theta = \frac{ED}{CD}$$

$$cos\theta = \frac{CE}{CD}$$

$$CE = CDcos\theta = xtan(90-\theta)cos\theta$$

$$Y_1 = Z - xsin\theta$$

$$Y_2 = Z - CE = Z - xtan(90 - \theta)cos\theta$$

Total distance travelled by right beam is;

$$Y_4 = Y_3 + Y_2$$

Transmittance of each beam is the function of distance travelled in the immersion fluid;

$$T_L = e^{-\alpha Y_1}$$

$$T_R = e^{-\alpha Y_4}$$

The contrast is then given by;

$$V = \frac{2\sqrt{I_1 I_2}}{I_1 + I_2} = \frac{2\sqrt{T_1 T_2}}{T_1 + T_2}$$

Appendix B

Fabrication steps used to make nanostructures.
Fabrication is done in NCSU Nanofabrication Facility (NNF), and Nanostructures and Nanomanufacturing Lab (NNL).

For Air

In NNF, spin coat Brewer Science ARC i-con-10.

Thickness = 109 nm (200 nm period)

Thickness = 97 nm (500 nm period)

Baked on a hot plate at 185 for 1min

In NNF, spin coat Sumitomo PFI-88A2 and PFI-88A5 photoresist.

Thickness = 200nm (200 nm period)

Thickness = 500nm (500 nm period)

Bake on hot plate at 95 for 1min

In NNL, expose square sample using Lloyd's mirror set-up

Dose = 65mJ (200 nm period)

Dose = 60mJ (500 nm period)

In NNF, develop photoresist.

Develop in MF-319 bath for 1min.

Rinse in DI water for 1 min

For DI water

In NNF, spin coat Brewer Science ARC i-con-IIL.

Thickness = 98 nm

Baked on a hot plate at 185 for 1min

In NNF, spin coat Sumitomo PFI-88-IILphotoresist.

Thickness = 50 nm

Bake on hot plate at 95 for 1min

In NNL, expose square sample using Lloyd's mirror set-up

Dose = 20mJ

In NNF, develop photoresist.

Develop in MF-319 bath for 1min.

Rinse in DI water for 1 min.

For Cargille Fluid 50350

In NNF, spin coat Brewer Science ARC i-con-IIL.

Thickness = 97 nm

Baked on a hot plate at 185 for 1min

In NNF, spin coat Sumitomo PFI-88-IILphotoresist.

Thickness = 50 nm

Bake on hot plate at 95 for 1min

In NNL, expose square sample using Lloyd's mirror set-up

Dose = 25mJ

Wash sample using water jet to remove oil

In NNF, develop photoresist.

Develop in MF-319 bath for 1min.

Rinse in DI water for 1 min.